

1 *Carbon dioxide removal efficiency of co-applied and*
2 *co-pyrolyzed feedstocks for enhanced rock weathering and*
3 *biochar in a sandy soil*

4 Authors: Maria-Elena Vorrath^{1*}, Johannes Meyer zu Drewen^{2,3,4}, Ingrid Smet⁵, Cierra Aldrich^{1,6},
5 Lennard Stoeck^{1,7}, Lara Feiertag¹, Sedrik Nauenburg¹, Ivo Neumann¹, Marvin Scherzinger⁸,
6 Theresa Siegmund⁸, Dirk Eifler⁹, Louise Foster¹, Niko Lahajnar¹, Jens Hartmann¹, Susanne
7 Hamburger¹⁰, Liam Adam Bullock¹¹, Silvia Placitu¹², Ruadhan Magee¹², Remi Rateau¹², Claudia
8 Kammann¹⁰, Mathilde Hagens¹³

9 ¹Department of Earth System Science, University of Hamburg, Germany

10 ²Ithaka Institute for Carbon Strategies, Goldbach, Germany

11 ³Agroscope, Zürich, Switzerland

12 ⁴Institute of Sustainable Energy Systems, Offenburg University, Offenburg, Germany

13 ⁵Carbon Drawdown Initiative, Fürth, Germany

14 ⁷Delft University of Technology, Delft, the Netherlands

15 ⁸Hamburg University of Technology, Hamburg, Germany

16 ⁹Chemistry Department of Chemistry, University of Hamburg, Germany

17 ¹⁰Hochschule Geisenheim University, Department of Applied Ecology

18 ¹¹Geological and Mining Institute of Spain, IGME C/Rios Rosas 23, Madrid, 28003, Spain

19 ¹²Silicate Carbon Limited

20 ¹³Soil Chemistry Group, Wageningen University & Research, Wageningen, the Netherlands

21

22 Highlights:

- 23 • Co-application of minerals and biochar provides the highest total carbon sink per
24 amendment mass
- 25 • Co-pyrolysis of biomass and mineral feedstocks enhances biochar stability
- 26 • Impregnation of biomass with magnesium increases biomass C_{org} conversion into biochar

- 27 • Thermal activation of serpentinised peridotite during pyrolysis accelerates weathering and
28 Mg release.
- 29 • Mineral-organic interactions reduce DOC leaching and support organic matter stabilization
30 in sandy soils.

31

32 Abstract

33 Enhanced rock weathering (ERW) and pyrogenic carbon capture and storage (PyCCS) are
34 promising land-based approaches for carbon dioxide removal (CDR), yet their co-deployment
35 remains poorly understood. This study investigates how co-application of minerals with
36 biochar and co-pyrolysing biomass with minerals influence mineral weathering, alkalinity
37 production, and carbon sequestration in a sandy soil with low cation exchange capacity (CEC)
38 and low organic carbon (C_{org}) content. We compared concrete, steel slag, basanite,
39 serpentinised peridotite, limestone and biochar as pure and co-applications, and
40 rock-enhanced biochars (RE-biochars) from dry-mixing and wet-impregnation of biomass and
41 consecutive co-pyrolysis. Downflow columns filled with amended sandy soil were incubated
42 for 75 weeks under elevated pCO_2 while monitoring cation fluxes, trace metal release,
43 dissolved organic carbon (DOC) dynamics, and changes in soil CEC. Wet-impregnation
44 substantially altered RE-biochar properties by increasing the pyrolysis carbon yield and
45 fraction of highly stable pyrogenic carbon particularly for Mg-rich feedstocks. Reduced DOC
46 losses and enhanced alkalinity production, attributed to mineral weathering as the geogenic
47 inorganic carbon sink (IC-Sink), was present for co-applications of biochar with basanite,
48 peridotite, and concrete. In contrast, RE-biochars mostly showed reduced geogenic IC-Sinks
49 for industrial materials, but increased geogenic IC-Sinks for peridotite from accelerated Mg^{2+}
50 release from thermally activated serpentine. Cation pool analyses revealed that most cations
51 were leached rather than being retained in exchangeable pools of the soil. Overall, our
52 evaluation of synergies arising from ERW-PyCCS combinations for terrestrial CDR highlights
53 material-specific advantages and trade-offs, supporting the recommendation of both single
54 application and co-application of biochar with mineral feedstocks.

55

56 Keywords: mineral-enhanced biochar, impregnation, RE-biochar, carbon dioxide removal,
57 pyrogenic carbon, biochar stability, climate change mitigation

59 1 Introduction

60 Limiting global warming and securing food production increasingly rely on land-based
61 strategies of carbon dioxide removal (CDR) (Shukla et al., 2022; Smith et al., 2024). Agriculture
62 contributed 13-21% of global anthropogenic greenhouse gas emissions between 2010 and
63 2019, also offers major potential for durable CDR through soil-based interventions (Babiker et
64 al., 2022; Nabuurs et al., 2022). Enhanced rock weathering (ERW) accelerates mineral
65 dissolution whilst converting atmospheric CO₂ into bicarbonate that can be stored for
66 millennia (Hartmann et al., 2013; Renforth, 2019), while pyrogenic carbon capture and storage
67 (PyCCS) stabilizes biomass carbon through pyrolysis, producing durable biochar (Schmidt et
68 al., 2025, 2019). Together, these methods offer long-term carbon sinks (C-Sinks) and
69 potentially improve agronomic performance (Schmidt et al., 2021; Vorrath et al., 2025),
70 offering valuable opportunities for climate mitigation amid widespread soil degradation and
71 increasing climate-related pressures on agriculture (Mbow et al., 2022; Nabuurs et al., 2022;
72 Shukla et al., 2022).

73 The performance of ERW and PyCCS is closely linked to soil health and nutrient cycling, both
74 of which are often impaired in degraded or drought-prone systems. Soil amendments that
75 enhance productivity while strengthening carbon storage could therefore accelerate the
76 adoption of these CDR approaches (Janssens et al., 2022; Waring et al., 2023). Biochar can
77 improve soil fertility, increase nutrient availability, enhance water retention, promote root
78 growth, and increase crop yields, particularly in tropical, highly weathered soils (Lehmann et
79 al., 2021; Schmidt et al., 2021), while also reducing soil nitrate leaching and N₂O emissions
80 (Borchard et al., 2019), immobilizing trace elements (Peng et al., 2018; Schmidt et al., 2021),
81 and supporting soil remediation efforts (Cornelissen et al., 2025; Wang et al., 2022). Enhanced
82 rock weathering can further raise soil pH, supply macro- and micronutrients, and enhance soil
83 structure (Beerling et al., 2018; Dupla et al., 2024; Haque et al., 2020; Swoboda et al., 2022).
84 During weathering, Mg²⁺- and Ca²⁺-bearing minerals react with atmospheric CO₂ to form
85 bicarbonate and increase soil alkalinity, reintroducing carbon into the geological cycle and
86 enabling its export to aquatic systems where it can be stored for millennia (Hartmann et al.,
87 2013; Renforth, 2019). Further, this process promotes secondary mineral formation in the soil
88 that stabilizes soil organic carbon (SOC) and protects labile biochar fractions (Buss et al., 2023;
89 Yang et al., 2021). These combined agronomic and biogeochemical effects highlight the need

90 to better understand the interactions between ERW and biochar and whether their combined
91 use can more effectively enhance long-term CDR while supporting resilient and productive
92 agricultural systems.

93 In addition to Ca²⁺- and Mg²⁺-rich silicate and carbonate rocks and industrial by-products, such
94 as steel slag or recycled concrete fines are increasingly explored as ERW feedstocks due to
95 their high reactivity, broad availability, and alignment with circular-economy principles
96 (McDermott et al., 2024; Renforth, 2019; Xu et al., 2024). However, weathering rates of all
97 feedstocks depend on multiple factors including water availability (Cipolla et al., 2022; Deng
98 et al., 2023), mineral speciation (Heřmanská et al., 2023, 2022), particle size and specific
99 surface area (Rinder and von Hagke, 2021), pCO₂ and soil pH (Amann et al., 2022),
100 temperature (Oelkers et al., 2018; Xu et al., 2024), and soil biota (Niron et al., 2024; Sohng et
101 al., 2025; Vicca et al., 2022). When combined with biochar which is composed of persistent
102 and semi-persistent carbon fractions (Keiluweit et al., 2010; Schmidt et al., 2022) that
103 undergoes gradual biotic and abiotic oxidation in soils after application (Pignatello et al.,
104 2024), these ERW feedstocks may further increase long-term carbon sequestration.

105 Interest in interactions between ERW and biochar has grown as co-application may enhance
106 water retention (Li et al., 2021; Sun and Lu, 2014), improve drainage (Vorrath et al., 2025),
107 increase soil pCO₂ through stimulated microbial activity (Palansooriya et al., 2019), increase
108 the soil cation exchange capacity (CEC) (Omara et al., 2023) or promote mineral-associated
109 organic matter (MAOM) formation (Buss et al., 2023; Han et al., 2020). Minerals may also
110 protect biochar from oxidation, thus reducing the decay of organic carbon (C_{org}) in the soil
111 (Nan et al., 2022). However, pot experiments have found only additive or modest synergistic
112 effects on ERW (Honvault et al., 2024; Te Pas et al., 2026). Beyond co-application, recent
113 studies show that adding minerals to biomass before pyrolysis to create rock-enhanced
114 (RE-)biochar has additional benefits (Meyer zu Drewer et al., 2025). Mg²⁺- and Ca²⁺-bearing
115 additives can enhance carbon retention, char aromatization, stability, and ash composition
116 (Buss et al., 2019; Grafmüller et al., 2022; Mašek et al., 2019; Nan et al., 2020), while thermal
117 treatment can alter the mineral surface area (Jiang et al., 2022; Mahanta et al., 2016), change
118 mineral speciation of e.g. serpentines (Du Breuil et al., 2019; Kelemen et al., 2011), or
119 passivate reactive surfaces by pyrogenic carbon coatings (Meyer zu Drewer et al., 2025).
120 Although some studies report unchanged pyrogenic carbon yields (Meyer zu Drewer et al.,

121 2025), others find increases after adding wood ash, potassium acetate, or rock powders (Buss
122 et al., 2019; Grafmüller et al., 2022; Mašek et al., 2019).

123 Despite recent advances, major uncertainties remain regarding the combined use of ERW and
124 PyCCS because most existing studies examine single materials in isolation, without
125 systematically comparing biochar, minerals, their co-application, and RE-biochars under
126 identical conditions on the same soil. Therefore, it is still unclear whether co-applying biochar
127 and rock powders enhances mineral dissolution, alkalinity export, or long-term CDR beyond
128 the largely additive effects observed so far (Honvault et al., 2024; Te Pas et al., 2026).
129 Additionally, little is known about how co-application influences soil solution chemistry,
130 dynamics of dissolved organic carbon (DOC), microbial processes, or the formation of
131 secondary minerals that could stabilize organic matter or retain cations (Buss et al., 2023). A
132 further unresolved issue is how to distinguish between alkalinity originating from mineral
133 weathering (geogenic) or biomass decomposition (biogenic), as cations from short-term
134 biogenic cycling do not contribute to additional CDR, while geogenic cations released through
135 ERW do (Vorrath et al., 2025). This is essential for accurate CDR accounting and assessing the
136 climate change-mitigation potential of mixed amendments. For co-pyrolysis, central
137 uncertainties for mineral feedstocks include whether thermal treatment accelerates or
138 suppresses weathering through changes in mineral structure, specific surface area, or surface
139 passivation (Mahanta et al., 2016; Meyer zu Drewer et al., 2025). Furthermore, interactions
140 with soil pCO₂, soil biota, trace metal mobility, and organo-mineral associations remain largely
141 untested in controlled soil systems. These uncertainties hinder the development of robust
142 monitoring, reporting and verification (MRV) frameworks and limit the ability to design
143 effective, scalable land-based CDR strategies.

144 This study examines how co-application and co-pyrolysis of various mineral feedstocks with
145 biochar influence mineral weathering, alkalinity production, and carbon sequestration in a
146 sandy, low-CEC, low-C_{org} soil. Under elevated CO₂ conditions (1-1.2 vol-% CO₂), we compared
147 pure applications of concrete, steel slag, basanite, peridotite, limestone, and biochar,
148 co-applications of biochar with mineral feedstocks, and eight RE-biochars (produced through
149 both dry-mixing and wet-impregnation) in a downflow soil column setup. The four objectives
150 of the study are:

- 151 1) to test two mineral-enhancement procedures: adding minerals either as dry rock powder
152 (dry-mixing) or suspended in water (wet-impregnation) to the biomass prior to pyrolysis,
153 and evaluate their impact on C_{org} conversion and carbon stability in RE-biochars;
- 154 2) to assess the development of the different C-Sinks from both ERW and PyCCS, cation and
155 trace metal release, and effects on soil organic carbon (SOC) and DOC of all applications
156 during a 75-week incubation experiment;
- 157 3) to identify possible synergistic effects of co-application and RE-biochars on mineral
158 weathering and trace metal retention; and
- 159 4) to determine the distribution of released cations between soil and leachate.
- 160 This work provides the first integrated assessment of combining diverse mineral feedstocks
161 with biomass for a joint CDR approach in soils, with relevance for land-based CDR scalability.

162

163 2 Materials and Methods

164 2.1 Materials and pyrolysis

165 2.1.1 Feedstocks

166 As biomass feedstock a mixture of wood chips from spruce, 0.8-1.1 mm (*Picea abies* L.) and
167 soybean meal, 0-0.5 mm (*Glycine max* L.) was utilized. The high oil content of the latter served
168 as a lubricant in the pelleting process. Mineral feedstocks included industrial materials of 1)
169 returned concrete, 0.5-1020 μm (provided by *Silicate Carbon Limited*), and 2) steel slag,
170 0.5-720 μm (*BaseLith* provided by *Thyssen Krupp*), and silicate rock of 3) basanite, 0.5-210 μm
171 (*Eifelgold* from *Rheinische Provinzial-Basalt- und Lavawerke GmbH & Co. oHG*) and 4)
172 serpentinised peridotite, 0.5-250 μm (*Dunite No.11* provided by *Sibelco*). Limestone, 0.5-2460
173 μm , was included as an additional control to compare amendments with the common farming
174 practice of liming. Additional details on the mineral feedstocks are provided in the
175 supplementary information, including grain size distribution (supplementary information S1)
176 and specific surface area (supplementary data D1), mineralogical and chemical composition
177 (supplementary data D2) and the thermogravimetric analysis of concrete and steel slag
178 (supplementary data D3).

179 2.1.2 Feedstock preparation

180 Pure biochar was produced from spruce chips and soybean meal in a 50:50 mass ratio.
181 Co-pyrolysis of biomass with minerals (biomass:mineral in a 70:30 mass ratio) was conducted
182 in two ways (Table 1). Feedstocks were either dry-mixed or wet-impregnated. For

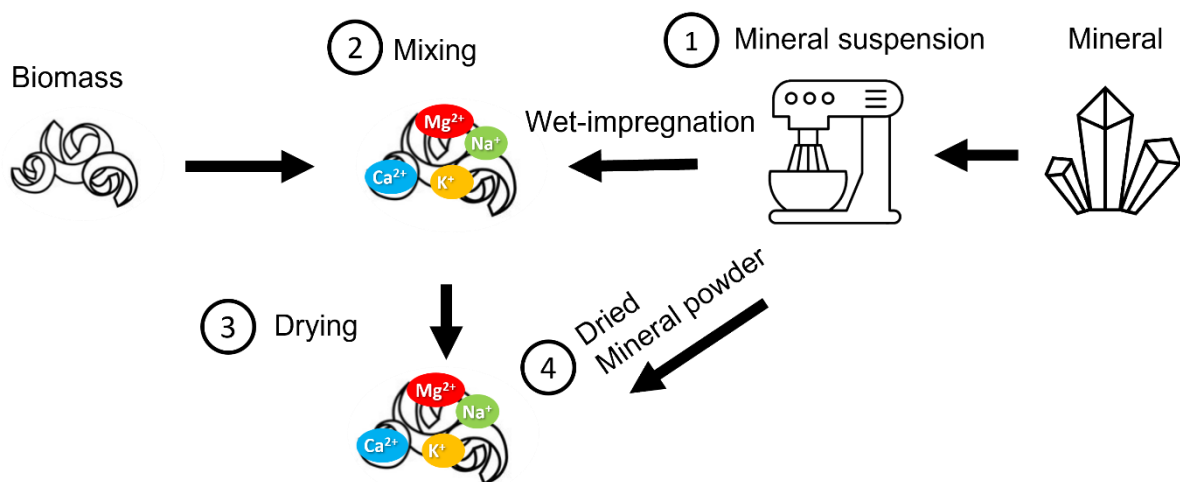
183 wet-impregnation, the feedstocks underwent a special processing, in which the biomass was
 184 soaked in a mineral suspension produced from the mineral feedstock to introduce dissolved
 185 cations into the biomass (Figure 1). The steps were:

- 186 1) Suspension of 2100 g mineral feedstock in 2 L deionized water (DI) to produce a cation
 187 enriched suspension. Stirring was facilitated by a Kitchen Aid (45 rpm, room temperature)
 188 to promote mineral dissolution and cation release of the minerals.
- 189 2) After five days, 4900 g of the spruce-soybean mix was soaked in the mineral suspension
 190 while the remaining mineral feedstocks were oven-dried (80 °C) separately.
- 191 3) The mixture was then air-dried at 20° C to evaporate the water.
- 192 4) The remaining mineral feedstocks added to the biomass afterwards.

193 Table 1: Configuration of biochar and rock-enhanced biochars.

No.	ID	Type	Mineral feedstock	Mass ratio biomass:mineral	Processing
1	ConcreteChar-dry	RE-biochar	Concrete	70:30	dry-mixed and co-pyrolyzed
2	ConcreteChar-wet	RE-biochar	Concrete	70:30	wet-impregnated and co-pyrolyzed
3	SteelslagChar-dry	RE-biochar	Steel slag	70:30	dry-mixed and co-pyrolyzed
4	SteelslagChar-wet	RE-biochar	Steel slag	70:30	wet-impregnated and co-pyrolyzed
5	BasaniteChar-dry	RE-biochar	Basanite	70:30	dry-mixed and co-pyrolyzed
6	BasaniteChar-wet	RE-biochar	Basanite	70:30	wet-impregnated and co-pyrolyzed
7	PeridotiteChar-dry	RE-biochar	Peridotite	70:30	dry-mixed and co-pyrolyzed
8	PeridotiteChar-wet	RE-biochar	Peridotite	70:30	wet-impregnated and co-pyrolyzed
9	Biochar	Biochar	none	100:0	pyrolyzed

194



195

196 Figure 1: Description of the processing of feedstocks for wet-impregnated RE-biochar. 1) The mineral
 197 feedstock is suspended in deionized water for 5 days and 2) the suspension is mixed with the biomass.
 198 3) After air-drying to evaporate the water from the biomass, the 4) remaining oven-dried mineral
 199 feedstock is added and mixed in as well.

200 All feedstock mixtures (dry-mixed and wet-impregnated) were pelleted to 6 mm on an
201 Amandus Kahl pellet press at the Hamburg University of Technology. Prior to pyrolysis, the dry
202 matter content of all feedstock pellets was determined at 105°C. The elemental composition
203 of raw feedstocks was analysed by Eurofins Umwelt-Ost GmbH, Germany (supplementary data
204 D4). Calculations of how much C_{org} converted into biochar (C_{org} conversion) and rock content
205 were conducted following the procedure described in Meyer zu Drewer et al. (2025).

206 All biochar and RE-biochars were pyrolyzed at 650 °C for approx. 15 min. in a PYREKA pyrolysis
207 unit by *Novocarbo* in Dörth, Germany (details described in supplementary information S2) and
208 their elemental compositions were analysed by Eurofins Umwelt-Ost GmbH, Germany,
209 following the guidelines of the European Biochar Certificate (EBC, 2024). Hydropyrolysis
210 (HyPy) was performed using the approach outlined by Meredith et al. (2017) (see
211 supplementary information S2) to determine the fraction of stable polycyclic aromatic carbon,
212 which contains more than 7 fused aromatic rings that exhibit high environmental stability
213 (Hagemann et al., 2025). This fraction is expressed as BC_{HyPy}, the stable fraction remaining of
214 the initial C_{org} content, and has a high probability to persist for >1000-years in soils, thus being
215 eligible as permanent CDR in the voluntary carbon market (Schmidt et al., 2025).

216 2.1.3 Soil

217 The soil utilized in the incubation experiments was sourced from an agricultural field in
218 Gartow, Germany, in March 2023, and had already been analysed by Ansari et al. (2026). The
219 soil is classified as a pure sand with a 93.8% sand fraction, a total carbon content of 1.24%
220 (1.2% C_{org}, 0.04% inorganic carbon, IC) and low CEC of 21.0 mmol kg⁻¹ (further details given in
221 supplementary information S3).

222 2.2 Incubation experiment and analyses

223 The incubation experiment was designed based on Vorrath et al. (2025) with 25 cm long
224 vertical soil columns. 500 g of sand soil was mixed with either 10 g of biochar pellets
225 (40.6 t ha⁻¹) and/or 9.9 g of loose mineral feedstocks (40.2 t ha⁻¹) or 15.0-16.3 g of RE-biochar
226 (60.9-66.2 t ha⁻¹) adjusted to contain 9.9 g of mineral feedstock per column. Each combination
227 was installed as duplicates. The experiment was conducted under elevated pCO₂ levels
228 corresponding to 1.0 ± 0.4 vol-% (box 1) and 1.2 ± 0.6 vol.-% (box 2), watered with CO₂ gasified
229 deionized water (equivalent to annual rainfall of 820 mm) over 75 weeks in a dark room at
230 around 22° C. Leachate samples were collected in weeks 2, 4, 6, 9, 15, 19, 27, 39, 51, 63 and
231 75 (further details described in supplementary information S4). After the experiment, the soil

232 CEC and exchangeable cations were measured on pooled samples from duplicates with the
233 same treatment.

234 At each sampling event, pH, temperature, and EC were measured immediately upon leachate
235 collection using a WTW 3630 IDS Multimeter. Dissolved inorganic carbon (DIC), total alkalinity
236 (TA), major ions, dissolved organic carbon (DOC), and dissolved silica (DSi) were subsequently
237 analysed. Trace metals were analysed on pooled leachate samples after weeks 9 and 27. The
238 parameters DIC, TA, major ions, DOC and DSi were additionally determined on the mineral
239 suspensions (all details in supplementary information S5). The CEC of soil after the experiment
240 was determined by Qmineral Analysis & Consulting (Belgium) using the ammonium acetate
241 saturation method of Kitsopoulos (1999), and major cations exchanged were quantified by
242 inductively coupled plasma atomic emission spectroscopy (ICP-OES). In carbonate-rich soils,
243 this extraction procedure can overestimate Ca^{2+} due to dissolution processes, whereas Mg^{2+} ,
244 Na^+ , and K^+ are not significantly affected (Lalitha et al., 2026). Therefore, because the Ca^{2+}
245 concentrations led to a cation balance with base saturation exceeding 100%, the cation
246 balance was adjusted by setting base saturation to 100%, which required recalculating the
247 Ca^{2+} value. The concentrations of Mg^{2+} , Na^+ and K^+ were not modified. Total carbon (C_{tot}), and
248 C_{org} of the soils before and after the experiment were determined following the method of
249 Nieuwenhuize et al. (1994), and IC was determined by subtracting C_{org} from C_{tot} (analytical
250 error <0.05%).

251 2.3 Key parameter calculations

252 To avoid an overestimation of organic alkalinity (Rieder et al., 2026), the IC-Sink was based on
253 carbonate alkalinity (CA) that was derived from measured values of DIC, pH, temperature, and
254 cation concentrations using PhreeqC (Parkhurst and Appelo, 2013) (database: phreeqc.dat).
255 The total carbon sink ($C\text{-Sink}_{\text{pot}}$) is the sum of the potential, stoichiometric sinks from
256 pyrogenic carbon ($\text{PyC-Sink}_{\text{pot}}$), based on the C_{org} provided by the biochar, and inorganic
257 carbon ($\text{IC-Sink}_{\text{pot}}$) as the maximum possible alkalinity provided by minerals and biomass upon
258 complete release. The same applies for actual measured C-, PyC- and IC-Sinks. The calculations
259 of all C-Sinks, the total chemical fluxes and CA production rates (CA_{prod}) of soil amendments
260 were adapted from Vorrath et al. (2025) (equations 1-8, supplementary information S6).
261 Values of the CA_{prod} after week 39 were used to extrapolate the duration of positive net fluxes
262 (compared to the control) and the corresponding degree of mineral weathering achieved at
263 this time (supplementary information S6). In general, values measured from the control were

264 subtracted from all other values to display the net fluxes. All C-sinks refer to one ton of soil
265 amendment.

266 To identify synergistic effects, we first determined the *expected* values of the total C-Sink and
267 IC-Sink by adjusting measured values of individual amendments according to the amount of
268 rock or biochar in each soil column. We then calculated the deviation of measured total C-Sink
269 and IC-Sink from the expected values (equations 9-11, details in supplementary information
270 S6). To determine the deviation between expected and measured geogenic IC-Sink, the cation
271 release and resulting IC-Sink from biochar was treated as a constant and the remaining IC-Sink
272 was attributed to mineral weathering (equation 12, supplementary information S6). Further,
273 the budgets of carbon and major cations in the soil were calculated to evaluate changes of
274 these budgets during the experiment (equations 13-16, supplementary information S6). For
275 trace metal fluxes, the deviation of measured from the expected fluxes were determined in
276 the same way as for the C-Sinks (equation 17, supplementary information S6).

277

278 3 Results

279 3.1 RE-biochar characterization

280 The basic properties of RE-biochars produced by dry-mixing and wet-impregnation, compared
281 to the pure biochar are shown in Table 2 (more details in supplementary data D5). The pure
282 biochar has a C_{org} content of 75.7% and H: C_{org} molar ratio of 0.30. Due to the weight loss of
283 biomass during pyrolysis the rock content of RE-biochars changed to 61.2-67.4% and show
284 consistently lower C_{org} (between 25.8-29.5%) and higher H: C_{org} ratios (between 0.45-0.56).
285 Pure biochar has a BC_{HyPy} content of 71.9 wt% C_{org} and a C_{org} conversion of 37.2%. For
286 RE-biochars, both BC_{HyPy} and C_{org} conversion range from 60.9-85.5 wt% C_{org} and 32.8-41.6 wt%
287 of biomass C_{org} , respectively. The highest C_{org} conversion (41.6 wt% C_{org}) and BC_{HyPy}
288 (85.5 wt% C_{org}) were reached by wet-impregnated basanite-enhanced RE-biochar and wet-
289 impregnated concrete-enhanced RE-biochar, respectively.

290 In the wet-impregnation procedure, using steel slag led to highest values of dissolved cations
291 in dry biomass (723.6 mg Ca^{2+} kg^{-1} and 136.2 mg Mg^{2+} kg^{-1}) while monovalent cations only
292 came from concrete (26.2 mg K^+ kg^{-1} biomass and 9.2 mg Na^+ kg^{-1} biomass) and basanite (19.3 mg
293 K^+ kg^{-1} and 11.3 mg Na^+ kg^{-1}) (Table 2, mineral suspension data in supplementary data D6).

294 Table 2: The basic characterization of pure biochar and RE-biochars from dry-mixing and
 295 wet-impregnation including the C_{org}, rock and biochar content, H:C_{org} molar ratio, the fraction of stable
 296 polycyclic aromatic carbon (BC_{HYPy}), biomass C_{org} conversion and the load of dissolved Ca²⁺, Mg²⁺, K⁺
 297 and Na⁺ per kilogram dry biomass added via mineral suspension within the wet-impregnation
 298 procedure. BC_{HYPy} and biomass C_{org} conversion values above the reference biochar are indicated in
 299 bold. Measurements based on n=1 representative sample.

	C _{org}	Rock	Biochar	H:C _{org} molar ratio	BC _{HYPy}	C _{org} conversion	Dissolved Ca ²⁺	Dissolved Mg ²⁺	Dissolved K ⁺	Dissolved Na ⁺
	%	wt%	wt%		wt%	wt%	mg k ⁻¹ biomass			
Biochar	75.7		100.0	0.30	71.9	37.2				
ConcreteChar-dry	28.2	62.9	37.1	0.55	81.8	36.4				
ConcreteChar-wet	25.8	65.5	34.5	0.56	85.5	36.4	17.9	0.0	26.2	9.2
SteelslagChar-dry	28.1	65.6	34.4	0.47	73.2	32.8				
SteelslagChar-wet	29.3	65.3	34.7	0.49	71.6	39.8	732.6	136.2	0.0	0.0
BasaniteChar-dry	28.5	64.6	35.4	0.51	72.6	40.4				
BasaniteChar-wet	26.1	67.4	32.6	0.51	79.0	41.6	8.6	6.7	19.3	11.3
PeridotiteChar-dry	29.5	62.1	37.9	0.53	60.9	34.0				
PeridotiteChar-wet	29.1	63.2	36.8	0.45	72.0	39.2	3.2	58.7	0.0	0.0

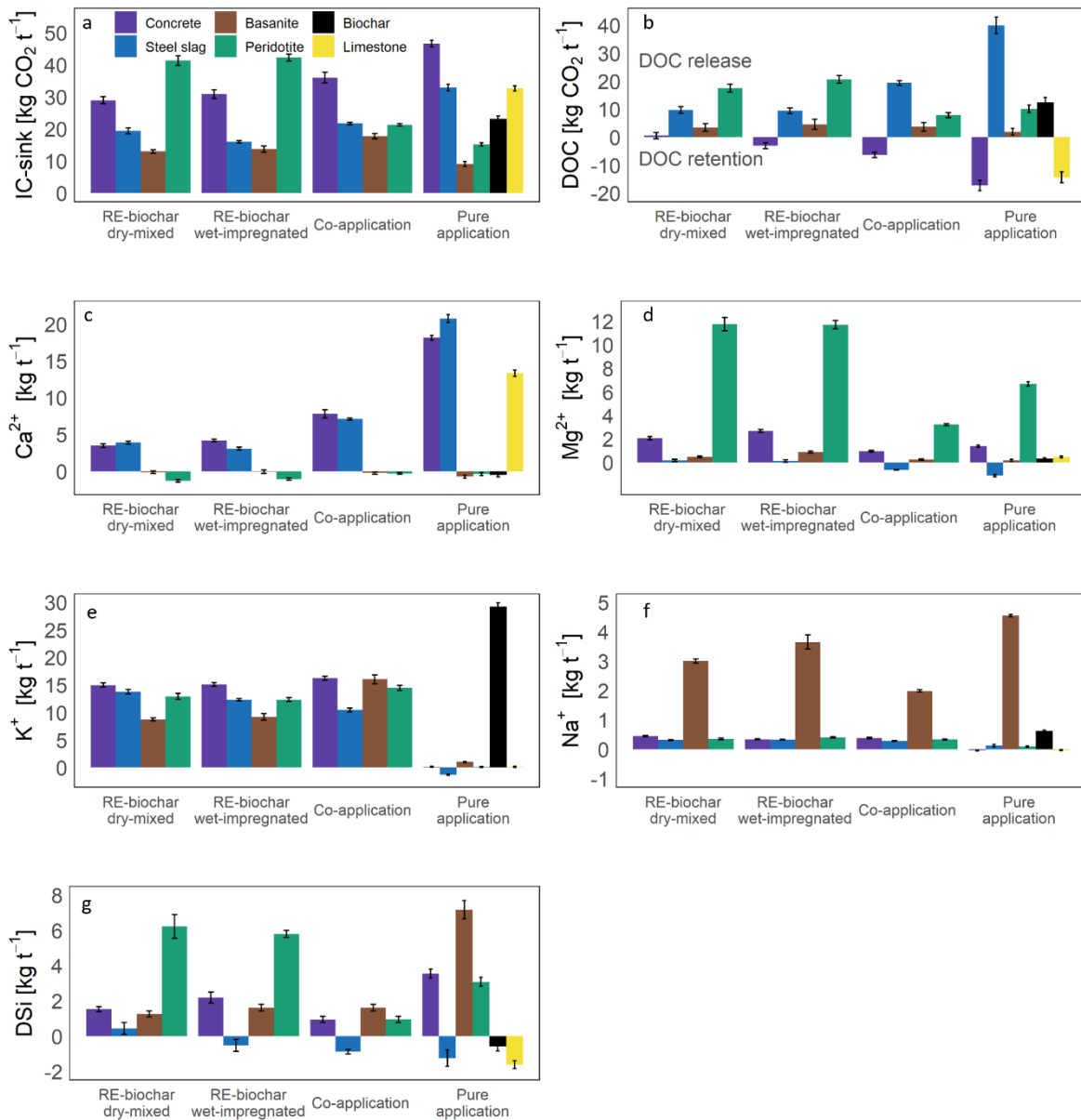
300

301 3.2 Leachate chemistry

302 3.2.1 Carbon and cation fluxes

303 The results of the total net fluxes are displayed in Figure 2, and show the CO₂ fluxes per ton of
 304 amendment for the IC-Sink and DOC, major cations and DSI (data in supplementary data D7).
 305 The IC-Sinks of silicates (basanite, peridotite) are the lowest, followed by limestone and
 306 industrial materials (concrete, steel slag), while the biochar IC-Sink is in the middle of this
 307 range (IC-Sink numbers see Table 6). In co-applications, IC-Sinks are balanced between the
 308 mineral feedstocks and the biochar, whereas in RE-biochars they are generally lower, with the
 309 exception of peridotite-based RE-biochars. Concrete and limestone amended columns show
 310 a net retention of DOC (14.7 kg CO₂ t⁻¹ for concrete and 12.2 kg CO₂ t⁻¹ for limestone), while
 311 silicates, steel slag and biochar release DOC (up to 33.9 kg CO₂ t⁻¹ for steel slag). Fluxes of Ca²⁺
 312 are highest for pure application of limestone and industrial materials (up to 20.8 kg t⁻¹), while
 313 biochar and amendments with silicates show a net retention of Ca²⁺ down to -1.3 kg t⁻¹. Mg²⁺
 314 fluxes are highest for all peridotite amendments, while RE-biochars with peridotite stand out
 315 with up to 11.7 kg t⁻¹ Mg²⁺. Net negative Mg²⁺ fluxes are present for applications of pure steel
 316 slag and its co-application with biochar. K⁺ fluxes are clearly dominated by biochar (20.2 kg t⁻¹)
 317 in all treatments, while the pure steel slag application shows a K⁺ retention of 1.3 kg t⁻¹. Na⁺
 318 fluxes are highest for amendments including basanite, with up to 4.5 kg t⁻¹. A retention of DSI

319 is observed in treatments of steel slag, pure biochar and limestone, while pure basanite,
 320 peridotite and concrete show highest release with up to 7.2 kg t⁻¹. Similar DSi fluxes also
 321 appear in RE-biochars with peridotite (up to 6.2. kg t⁻¹).



322
 323 Figure 2: Total net fluxes over 75 weeks calculated from the experiment of a) the IC-Sink, b) dissolved
 324 organic carbon (DOC), c) calcium (Ca²⁺), d) magnesium (Mg²⁺), e) potassium (K⁺), f) sodium (Na⁺), and
 325 g) dissolved silica (DSi). The units refer to one ton of material (or material combination). Error bars
 326 indicate standard deviation (n=2).

327
 328 The extrapolation of weekly CA_{prod} shows continued positive CA_{prod} fluxes between 160 and
 329 2022 weeks (i.e. 3 to 39 years) after the end of the experiment (Table 3). This leads to a

330 complete dissolution of concrete, while only 2.6-9.1% of the IC-Sink_{pot} of the other
 331 amendments would be realized.

332 Table 3: The extrapolation of positive alkalinity fluxes based on experimental data from pure mineral
 333 amendments with the experimental IC-Sink, the maximum positive alkalinity production based on a
 334 linear extrapolation and the resulting extrapolated IC-Sink. The sum of both IC-Sinks is taken to display
 335 the released IC-Sink based on the individual IC-Sink potential. The extrapolation for concrete had to be
 336 cut off in week 2022 as the IC-Sink_{pot} reached 100%.

Mineral	Experimental IC-Sink	Maximum positive alkalinity production	Extrapolated IC-Sink	Summed IC-Sink	IC-Sink potential	Released IC-Sink
	kg CO ₂	weeks	kg CO ₂	kg CO ₂	kg CO ₂	%
Concrete	46.6	2022	670.0	716.6	716.7	100.0%
Steel slag	32.9	160	12.0	44.9	774.8	5.8%
Basanite	9.0	524	22.2	31.2	450.6	6.9%
Peridotite	15.2	234	6.8	22.0	998.8	2.2%
Limestone	32.6	390	44.7	77.2	851.8	9.1%

337

338 3.2.2 Trace metal fluxes and retention

339 Trace metal concentrations declined markedly between week 9 and week 27 (details in
 340 supplementary information S7 and supplementary data D8). Several RE-biochars, particularly
 341 those containing steel slag or peridotite, as well as single biochar, showed elevated releases
 342 of cadmium, chromium, copper, lead, and nickel, in some cases exceeding German Drinking
 343 Water Ordinance limits. Exceedances were also observed for certain co-applications and even
 344 in the control soil for nickel and lead during the first sampling period.

345 Trace metal retention was determined for the first sampling interval and varied substantially
 346 among the different soil amendments, with notable differences between RE-biochars and
 347 their respective co-applications (

348 Table 4, supplementary information S6, eq. 17). Overall, 60% of the co-applications showed
 349 clear retention, whereas RE-biochars displayed limited retention or even increased releases.
 350 The strongest and most consistent retention across metals was observed for concrete
 351 RE-biochars, which retained up to and above 100% for several elements (Cr, Cu, Ni). Peridotite
 352 amendments showed mixed effects, with high retention of Cr and Ni in RE-biochars and
 353 retention of Cd, Cu, and Pb in the co-application. Basanite and steel slag amendments had
 354 retained several trace metals except for Ni. In general, Cu retention was evident in all co-

355 applications. These deviations from expected values underline that trace metal retention is
 356 highly amendment-specific, with synergistic effects in co-applications evident in some cases
 357 but absent or even counterproductive in others.

358 Table 4: The deviation of trace metal fluxes from measured to expected net values (%) in
 359 mineral-biochar co-applications and co-pyrolysis of biomass with minerals based on dry-mixing and
 360 wet-impregnation. Green fields indicate a retention of trace metals.

Configuration	Cd	Cr	Cu	Ni	Pb
ConcreteChar-dry	26.64	< -100	-53.16	> 100	13.88
ConcreteChar-wet	39.66	< -100	-31.26	< -100	2.13
Concrete + Biochar	< -100	13.94	< -100	< -100	> 100
SteelslagChar-dry	85.34	> 100	68.70	> 100	79.36
SteelslagChar-wet	87.86	> 100	72.87	91.63	83.39
Steel slag + Biochar	> 100	-13.36	< -100	36.63	< -100
BasaniteChar-dry	35.57	> 100	14.21	> 100	7.94
BasaniteChar-wet	48.18	-6.76	23.02	> 100	25.27
Basanite + Biochar	-22.20	> 100	-41.02	> 100	-49.67
PeridotiteChar-dry	40.17	> 100	21.83	< -100	32.18
PeridotiteChar-wet	47.69	< -100	22.83	< -100	35.96
Peridotite + Biochar	-57.11	93.26	-97.66	6.14	-71.33

361

362 3.2.3 Soil cation budgets

363 The cation budget, after correction for the control soil, represents the distribution pathways
 364 of cations that were released from the input materials either to the exchangeable fraction or
 365 the leachate water (Table 5, figure in the supplementary information S8 and supplementary
 366 data D9). In general, 2.2-14.7% of cations from the input materials are present in the leachate
 367 water and 0.2-2.1% in the exchangeable fraction, for a total of 2.6-15.9% of mobilized cations.
 368 The pure biochar amendment is a clear exception that released 57.8% of its major cations to
 369 the leachate and 2.0% to the exchangeable fraction. A redistribution of soil inherent cations
 370 during the experiment (from soil mineral dissolution and immobilization) may be masked by
 371 cations from input materials. However, some values are above 100% or below -100%, which
 372 is a clear indicator of the involvement of cations other than from the input material. Taking
 373 into account the maximum possible stoichiometric cation release, between 84.1 and 98.6% of
 374 major cations remain in the input material (or other solid soil pools), with an exceptional
 375 cation release of 65.7% from pure biochar. Negative values indicate a loss of the specific cation
 376 from either the exchangeable fraction or leachate.

377 Table 5: The net cation budget of the soil determined related to the input material (%) from cations in
 378 the soil exchangeable fraction and leachate. Cells with “+” and “-” are cases where specific cations
 379 were not added by the input material but positive or negative net values appeared in the samples,
 380 respectively. Green fields present values above 100%, indicating mobilized cations from the soil, grey
 381 fields are negative values that indicate the retention of cations in the soil. To avoid an overestimation
 382 of cation release from the input materials, values of K⁺ and Na⁺ above 100% were set to 100% of the
 383 input material to calculate the corrected remaining material.

Configuration	ConcreteChar-dry	ConcreteChar-wet	Concrete + Biochar	Concrete	SteelslagChar-dry	SteelslagChar-wet	Steel slag + Biochar	Steel slag	BasaniteChar-dry	BasaniteChar-wet	Basanite + Biochar	Basanite	PeridotiteChar-dry	PeridotiteChar-wet	Peridotite + Biochar	Peridotite	Biochar	Limestone
Exchangeable cations %																		
Ca2+	0.2	-0.1	1.1	1.2	0.0	0.3	0.5	0.4	-0.1	0.6	0.3	0.3	-25.0	-26.8	-11.6	-187.0	-6.2	0.9
Mg2+	2.7	0.4	2.8	0.7	2.1	1.6	4.2	1.3	0.6	1.2	2.0	0.5	0.2	0.2	0.4	0.1	18.1	-2.3
K+	4.2	18.9	-4.2	-32.9	24.5	9.3	19.2	+	-0.5	0.0	0.4	1.9	50.3	57.2	21.9	2553.0	13.3	-88.4
Na+	113.6	0.2	120.2	1050.2	487.4	117.4	0.2	+	7.0	0.0	3.4	0.0	-1099	-1411	-99.0	-	-148.4	+
Sum	1.0	0.5	1.5	2.1	1.6	0.9	1.8	1.5	0.7	0.8	1.2	0.4	0.2	0.3	0.3	0.3	2.0	1.2
Leached cations %																		
Ca2+	1.5	1.7	4.2	5.4	1.3	1.0	3.7	5.9	-0.6	-0.3	-0.7	-0.9	-14.4	-12.7	-3.3	-22.1	-3.1	3.1
Mg2+	15.1	19.3	8.1	8.2	0.1	-0.1	-3.9	-4.4	1.1	2.1	0.6	0.3	6.6	6.3	2.1	2.3	3.7	13.2
K+	193.6	207.8	166.1	14.4	208.4	184.2	110.9	-	54.0	57.6	96.5	6.3	175.5	171.3	155.1	59.5	158.8	19.4
Na+	106.6	84.6	75.9	-17.1	140.0	141.8	66.7	+	41.4	48.5	31.3	38.2	520.3	773.5	80.9	+	75.0	-
Sum	10.0	10.2	13.3	5.7	6.8	6.0	7.7	4.4	9.4	10.6	14.7	3.6	10.4	10.0	7.7	2.2	57.8	3.3
Released cations %																		
Ca2+	1.7	1.6	5.3	6.6	1.3	1.4	4.2	6.3	-0.6	0.3	-0.4	-0.6	-39.4	-39.5	-14.8	-209.2	-9.3	4.0
Mg2+	17.8	19.7	10.9	8.9	2.2	1.5	0.4	-3.0	1.8	3.3	2.7	0.7	6.8	6.5	2.5	2.4	21.9	10.9
K+	197.8	226.7	162.0	-18.5	232.9	193.4	130.1	+	53.5	57.6	96.9	8.2	225.8	228.5	176.9	2612.5	172.1	-69.0
Na+	220.2	84.9	196.0	1033.1	627.4	259.2	66.9	+	48.3	48.5	34.7	38.3	-579.0	-637.9	-18.1	-	-73.4	+
Sum	11.0	10.8	14.8	7.7	8.4	6.9	9.5	5.8	10.1	11.4	15.9	4.1	10.6	10.3	8.1	2.6	59.8	4.5
Corrected remaining material %																		
	92.9	93.3	88.8	93.2	95.9	95.8	91.8	94.2	89.9	88.6	84.1	95.9	92.6	92.8	94.8	98.6	65.7	96.0

384

385 3.3 C-Sinks from different soil amendments

386 The total C-Sink_{pot} ranges between 451 and 2801 kg CO₂ t⁻¹ for basanite and biochar,
 387 respectively (Table 6). Biochar provides the highest C-Sink_{pot} due to high C-Sink:mass ratio with
 388 2801 kg CO₂ t⁻¹ of biochar, while the mass-based C-Sink_{pot} of mineral feedstocks is generally
 389 lower at 383 to 999 kg CO₂ t⁻¹ material. Co-applications achieve a C-Sink_{pot} of 1632 to 1904 kg
 390 CO₂ t⁻¹ whilst RE-biochars range from 1261 to 1697 kg CO₂ t⁻¹ material.

391 The experimentally determined actual C-Sinks based on the calculated PyC-Sink and IC-Sink
 392 from leachate water analyses ranges from 9.0 kg CO₂t⁻¹ (basanite) to 46.6 kg CO₂ t⁻¹ (concrete)
 393 for pure mineral amendments but increases to around 1038 kg CO₂ t⁻¹ for co-applications and
 394 to 874.4 kg CO₂ t⁻¹ for RE-biochars (Table 6). The deviation of the measured from the expected
 395 total C-Sink is between -1.7 and 0.2% for RE-biochars and co-applications, except for
 396 RE-biochars with peridotite, where the measured C-Sink is 3.4% higher. In RE-biochars, the
 397 measured IC-Sinks are lower than the expected IC-Sinks calculated according to the pure
 398 amendments, by -45.9 to -19.9%. Only the IC-Sink of the wet-impregnated basanite RE-biochar
 399 is increased by 0.7% and peridotite RE-biochars stand out with a 127.6% and 133.6% higher
 400 IC-Sink for dry-mixing and wet-impregnation, respectively. Except for steel slag (-22.6%),
 401 co-applications also show an up to 11.1% higher measured IC-Sink. The deviation for the
 402 geogenic IC-Sink or the value of accelerated/suppressed weathering is similar, with negative
 403 values of -63 to -17.6% for RE-biochars and the co-application with steel slag, while the other
 404 RE-biochars and co-applications are positive, with peridotite RE-biochars showing remarkable
 405 accelerated values of up to 251.7%.

406 Table 6: The C-Sink potentials and actual C-Sinks from the experiment of all RE-biochars, co-
 407 applications and pure amendments are reported as the C-Sink, the inorganic carbon sink (IC-Sink) and
 408 the pyrogenic carbon sink (PyC-Sink). The deviation of the measured from the expected C-Sinks and
 409 IC-Sinks is expressed as percentage. The deviation of the measured from expected geogenic IC-Sink
 410 refers to the IC-Sink solely occurring from mineral weathering (calculated after equations 9-12,
 411 supplementary information S6).

	Column Material	C-Sink potential			C-Sink from experiment			Deviation		
		C-Sinkpot	IC-Sinkpot	PyC-Sinkpot	C-Sink	IC-Sink	PyC-Sink	C-Sink	IC-Sink	Geogenic IC-Sink
		kg CO ₂ t ⁻¹			kg CO ₂ t ⁻¹			%		
RE-biochar	ConcreteChar-dry	1657.2	623.2	1034.0	874.4	28.9	845.4	-1.0	-23.7	-30.5
	ConcreteChar-wet	1597.0	651.0	946.0	839.4	30.9	808.5	-0.9	-19.9	-25.0
	SteelslagChar-dry	1575.1	544.8	1030.3	773.6	19.4	754.2	-1.3	-34.2	-46.8
	SteelslagChar-wet	1627.5	553.2	1074.3	785.5	16.0	769.6	-1.7	-45.9	-63.0
	BasaniteChar-dry	1328.5	283.5	1045.0	771.5	13.0	758.5	-0.1	-28.4	-17.6
	BasaniteChar-wet	1261.4	304.4	957.0	769.8	13.7	756.1	0.0	0.7	1.6
	PeridotiteChar-dry	1697.0	615.3	1081.7	700.1	41.4	658.7	3.4	127.6	245.7
	PeridotiteChar-wet	1691.0	624.0	1067.0	810.0	42.3	767.7	3.1	133.6	251.7
Co-application	Concrete + Biochar	1763.9	369.1	1394.8	1038.3	36.0	1002.3	0.1	3.3	5.0
	Steel slag + Biochar	1792.8	398.0	1394.8	1024.0	21.7	1002.3	-0.6	-22.6	-38.4
	Basanite + Biochar	1631.5	236.7	1394.8	1020.0	17.7	1002.3	0.2	10.4	37.1
	Peridotite + Biochar	1904.2	509.4	1394.8	1023.5	21.2	1002.3	0.2	11.1	27.9
Pure	Concrete	716.7	716.7	0.0	46.6	46.6	-			

Steel slag	774.8	774.8	0.0	32.9	32.9	-
Basanite	450.6	450.6	0.0	9.0	9.0	-
Peridotite	998.8	998.8	0.0	15.2	15.2	-
Biochar	2800.6	24.9	2775.7	1994.5	23.1	1994.5
Limestone	851.8	851.8	0.0	32.6	32.6	-

412

413 4 Discussion

414 4.1 Impact of co-pyrolysis on C_{org} conversion and biochar stability

415 Our results demonstrate that increases in C_{org} conversion in RE-biochars prepared with
416 wet-impregnation of biomass are correlated to Mg^{2+} concentrations in the mineral
417 suspension, following a strong exponential relationship ($r^2=0.9984$, supplementary
418 information S9). Wet-impregnation with steel slag produces the highest increase of C_{org}
419 conversion (7.0%) after adding 0.014 wt% of dissolved Mg^{2+} to the dry biomass prior to
420 pyrolysis (Table 2). This aligns with several studies showing that dry-mixing with magnesium
421 before pyrolysis markedly enhances carbon retention in biochar. For example, Zhu et al.
422 (2023) report that 1 wt% Mg^{2+} (as $MgCl_2$) increases C_{org} conversion by more than 12%, which
423 is likely attributed to the catalytic role of Mg^{2+} in suppressing volatile formation during thermal
424 decomposition (Yu et al., 2014). Higher C_{org} conversion has also been linked to the formation
425 of MgO and magnesium carbonate phases that sorb small (volatile) low molecular weight
426 carbon compounds and form protective barriers against oxidation (Nan et al., 2020).
427 Compared to other cations, Mg^{2+} consistently appears as the most effective additive for
428 improving C_{org} conversion (Nan et al., 2020). Although Ca^{2+} has also been associated with
429 increased carbon content (Li et al., 2014), no significant effect was detected in this study.

430 Despite the strong influence of Mg^{2+} in wet-impregnated treatments, the pure biochar still
431 shows a higher C_{org} conversion (37.2%) than RE-biochars with concrete or dry-mixed
432 RE-biochars with steel slag and peridotite (Table 2). Peridotite contains the highest amount of
433 MgO (45.6 wt%) present mainly in the minerals olivine and serpentine, however, the
434 corresponding dry-mixed RE-biochar has a low C_{org} conversion efficiency. Likely, the form of
435 Mg^{2+} , either bound within a crystal lattice of a mineral or dissolved in water, plays a crucial
436 role affecting Mg^{2+} catalytic activity. Basanite derived RE-biochars show a generally higher C_{org}
437 conversion, independent from the mixing procedure, which is controversial to other studies
438 (Meyer zu Drewer et al., 2025).

439 Previous studies suggested increases in C_{org} stability when biomass was co-pyrolyzed with
440 mineral additives, but consistent experimental evidence has been lacking (Buss et al., 2022;
441 Meyer zu Drewer et al., 2025, submitted). In our study, hydrolysis revealed a higher
442 percentage of BC_{HyPy} for most RE-biochars except those mixed with peridotite (Table 2**Fehler!**
443 **Verweisquelle konnte nicht gefunden werden.**). Although the high Ca content in concrete
444 (41.7 wt% CaO) can be clearly associated with higher BC_{HyPy} , this relationship is not present
445 for steel slag, despite its similarly high Ca content (45.1 wt% CaO). We propose that this
446 contrast may stem from different minerals containing the bulk of the calcium, which is calcite
447 for the concrete and Ca-silicates, oxides and hydroxides for the steel slag (supplementary data
448 D2). Although concrete mainly contains calcium carbonates that may decompose during
449 pyrolysis, our thermogravimetric analysis did not show decarbonation that would have made
450 CaO available to promote carbon stabilization (supplementary data D3). The only mineral that
451 could have provided CaO during pyrolysis is portlandite, but its content was likely too low
452 (0.2%) to have a substantial effect on biochar stabilization. In steel slag, calcium is
453 predominantly found in the form of calcium silicates and calcium iron oxides, which likely
454 remain inert during pyrolysis and therefore do not influence carbon stability. Conversely, steel
455 slag also contains 10.2% portlandite, yet this comparatively high abundance still does not
456 enhance C_{org} stability, directly contradicting our earlier expectation that portlandite-derived
457 CaO would increase biochar stabilization. However, our results regarding concrete RE-biochars
458 fit earlier findings showing that calcium carbonates promote carbon stabilization attributed to
459 matrix aromatization during pyrolysis (Li et al., 2014), while the effects of calcium silicates,
460 calcium iron oxides, and calcium hydroxides remain unresolved.

461

462 4.2 C-Sinks from different soil amendments in a sandy soil

463 4.2.1 IC-Sinks from mineral weathering

464 The IC-sinks developing from pure mineral amendments and based on leachate analyses,
465 show a realization of 1.5% (peridotite) to 6.5% (concrete) of the stoichiometric IC-Sink_{pot} over
466 17 months with the order of fastest weathering being: concrete > steel slag > limestone >
467 basanite > peridotite (Table 6). Fast weathering can mainly be attributed to the presence of
468 the minerals calcite (concrete, steel slag, limestone), portlandite and larnite (steel slag),
469 nepheline and leucite (basanite) and olivine (peridotite, basanite). A similar order has been
470 found by Hammes et al. (2025) in a large-scale greenhouse pot experiment, where only the

471 order of basanite and peridotite were reversed. The release of 4.2% IC-Sink_{pot} from steel slag
472 is comparable to previous findings under similar conditions, where 1.6% of the IC-Sink_{pot} was
473 released over 15 months in a plant-inclusive pot experiment (Steinwidder et al., 2026).
474 Peridotite shows a lower release compared to a 2-month pot experiment, where values were
475 3.4 times higher (Te Pas et al., 2026). An ERW field study using returned concrete in Ireland
476 yielded up to 2.7% of the IC-sink_{pot} over 11 months, including plants and non-carbonic acid
477 weathering contributions (McDermott et al., 2024). Many pot and mesocosm studies report
478 low to negligible alkalinity release from basaltic amendments due to unfavourable water
479 conditions, plant presence, or soil–cation interactions (Buckingham and Henderson, 2024;
480 Steinwidder et al., 2026; Vienne et al., 2026b, 2024, 2022).

481 Our 17-month experiment enabled us to observe stabilized CA_{prod} fluxes (after week 39) and
482 extrapolate the continuation of these fluxes (Table 3). Although we acknowledge that a linear
483 model does not fully capture the complexity of mineral weathering in the soil, it provided the
484 best fit for our measured fluxes (supplementary information S6, Table S2) which means the
485 resulting extrapolation should not be viewed as definitive. While concrete would have been
486 completely weathered after 40 years, steel slag, basanite, peridotite, and limestone would
487 have released 2.2-9.1% of their IC-sink_{pot} until CA_{prod} fluxes were equal to the control. This
488 suggests that, under most conditions, the full IC-sink_{pot} is unlikely to convert into an actual,
489 long-term C-sink. Losses can generally occur due to secondary mineral formation (Dietzen and
490 Rosing, 2023; Niron et al., 2024; Steinwidder et al., 2026; Te Pas et al., 2026, 2025), plant
491 uptake of cations (Kantola et al., 2023; Rijnders et al., 2023; Vienne et al., 2026a), cation
492 sorption to organic surfaces and MAOM formation (Buss et al., 2024; Te Pas et al., 2026;
493 Vienne et al., 2026a), and mineral surface passivation (Oelkers et al., 2018). These alternative
494 cation pathways illustrate uncertainties in their contribution to alkalinity generation.

495 4.2.2 C-Sink from biochar and combined applications

496 In biochar, the main contributor of the total C-sink_{pot} originates from the PyC-sink, whereas
497 its IC-sink is minor and does not contribute additional carbon sequestration, and therefore no
498 CDR (Vorrath et al., 2025). While IC-sinks from minerals develop slowly, more than 93% of the
499 biochar IC-sink is released after week 75 (and 98% after week 87) (Table 6). As minerals have
500 relatively small C-Sink_{pot}:mass ratios, the C-Sink_{pot} of co-applications and RE-biochars is
501 defined by the contributions of each material, but not proportional to the biochar content.
502 For example, the 1:1 co-application of basanite and biochar provides a C-sink_{pot} of 1631 kg

503 CO₂ t⁻¹, about 300 kg CO₂ t⁻¹ higher than the corresponding RE-biochars containing 34 wt%
504 biochar. On the other side, a 1:1 co-application also exceeded the corresponding RE-biochar
505 C-sink_{pot} by 110-170 kg CO₂ t⁻¹ although the biochar content was 69 wt% (Vorrath et al., 2025).
506 This indicates that the pyrogenic carbon contribution in RE-biochars is lower than its
507 proportional share. Although wet-impregnated feedstocks show higher C_{org} conversion rates
508 (Table 2), the variability of C_{org} across materials prevents clear attribution of potential effects
509 of mixing procedures on the C-sink_{pot} or experimental C-sink.

510 In contrast to mineral weathering, where the IC-sink increases over time, the PyC-sink of
511 biochar decreases due to decomposition of labile organic carbon fractions (Azzi et al., 2024;
512 Sanei et al., 2025). Our BC_{HyPy} content of 71.9% of C_{org} (Table 2) is low compared to typical
513 values of woody biochars and RE-biochars at 650 °C (BC_{HyPy} above 90%) (Meyer zu Drewer et
514 al., 2025). Biochar stability is strongly influenced by feedstock composition (Ippolito et al.,
515 2020), with lignin-rich biomasses producing more stable biochars (Ma et al., 2019). Thus, the
516 use of protein-rich soybean meal (Karr-Lilienthal et al., 2004) alongside spruce in our study
517 likely explains the lower stability observed here. Nevertheless, over longer timescales,
518 decreases in the PyC-sink may be partially offset by increases in the IC-sink, resulting in a
519 complementary and sustainable CDR portfolio (Meyer zu Drewer et al., submitted; Rueda et
520 al., 2021; Vorrath et al., 2025). Overall, co-application appears more practical and economical
521 because of fewer production steps and offers a high C-sink_{pot} per mass, while co-pyrolysis can
522 increase C_{org} stability.

523

524 4.2.3 Synergistic effects on the total C-Sink and the role of geogenic cations
525 Expected C-sinks based on pure amendments were compared with experimental outcomes to
526 evaluate synergistic/antagonistic effects (Table 6). For both co-applications and RE-biochars,
527 the deviation of measured from expected total C-sink remains below 3.4%, indicating limited
528 synergistic or antagonistic effects from combining geochemical and pyrogenic CDR. The
529 deviation of the measured IC-sink only captures deviations from combined mineral
530 weathering and pyrogenic carbon, while the deviation of the measured geogenic IC-Sink
531 indicates whether mineral weathering itself is accelerated or reduced. Both metrics show
532 consistent patterns: in RE-biochars, combinations with concrete, steel slag, and dry-mixed
533 basanite result in reduced IC-sinks; wet-impregnated basanite does not alter the IC-Sink; and
534 peridotite RE-biochars show remarkably higher IC-Sinks. In co-applications, the IC-sinks are

535 enhanced for concrete, basanite, and peridotite, whereas steel slag shows a reduced IC-sink.
536 These results demonstrate that simple addition of IC-sinks from single mineral powder and
537 biochar applications does not accurately mirror the actual leaching of major cations measured
538 in RE-biochars.

539 However, since more than 90% of biochar's IC-sink was released within 17 months (Table 6),
540 the geogenic IC-sink in combined amendments can be conservatively estimated by simply
541 subtracting the biochar IC-sink_{pot.} Previous studies reported no increase in IC-sinks for
542 co-applications of biochar and basanite (Honvault et al., 2024; Vorrath et al., 2025), while
543 slight increases were observed for peridotite (Te Pas et al., 2026). Such comparisons of
544 synergistic effects across different soils remain difficult as effects are found to be strongly soil-
545 dependent (Hammes et al., 2025; Vorrath et al., in prep.). For RE-biochars, suppressed mineral
546 weathering due to pyrogenic coatings on mineral surfaces has been hypothesised (Meyer zu
547 Drewer et al., 2025) but not experimentally confirmed (Meyer zu Drewer et al., submitted).
548 CaO production via thermal alteration of minerals in steel slag and concrete is also unlikely, as
549 our thermogravimetric analyses showed weight loss that can be mainly attributed to a loss of
550 water (supplementary data D3). In contrast, the substantially higher measured geogenic
551 IC-sink of peridotite RE-biochars (up to +251.7%) can be explained by thermal activation of
552 serpentine minerals during pyrolysis (see chapter 4.3.3). In most co-applications (except for
553 steel slag), our observations indicate that sorption surfaces introduced by biochar addition do
554 not delay or reduce the IC-sink by cation scavenging from soil solution (Planavsky et al., 2024).
555 Instead, they support the concept that biochar improves weathering conditions (Amann and
556 Hartmann, 2019; Meyer zu Drewer et al., 2025; Vorrath et al., 2025). The strong decrease of
557 steel slag weathering in the co-application may be linked to interactions between dissolved
558 calcium silicates and pyrogenic carbon (see chapter 4.4).

559 Considering these synergistic patterns, a qualitative assessment of the different materials
560 suggests that single applications and co-applications of biochar with all mineral feedstocks
561 offer the most promising performance in the studied sandy soil (supplementary information
562 S10). These combinations align with the experimentally observed enhancement of measured
563 geogenic IC-Sinks for concrete, basanite and peridotite co-applications, and benefit from
564 biochar's capacity to retain DOC and improve weathering conditions (Figure 2). Overall, the
565 substantial reduction of DOC leaching with pure concrete and in co-application with biochar
566 could counterbalance possible CO₂ efflux effects from non-carbonic acid weathering (West

567 and McBride, 2005). In contrast, RE-biochars combined with steel slag or basanite appear less
568 favourable, as they tend to suppress mineral weathering and do not mitigate DOC losses,
569 despite the strong thermally activated weathering observed for peridotite RE-biochars.

570 Although trace metal release was not included in this qualitative evaluation, it remains a
571 relevant consideration for field deployment and must be assessed in relation to local soil
572 conditions and regulatory thresholds. Overall, these observations highlight that the suitability
573 of individual minerals depends not only on their IC-Sink_{pot} but also on their interactions with
574 biochar and their broader effects on soil carbon dynamics and practical implementation.

575 Combining ERW and biochar in field applications introduces challenges for monitoring,
576 reporting, and verification (MRV) because the two approaches rely on fundamentally different
577 accounting procedures. Biochar MRV is based on pre-deployment chemical and physical
578 characterisation (e.g. Schmidt et al., 2024), while ERW monitoring requires long-term analyses
579 of soil or leachate samples to quantify mineral dissolution and carbon sequestration (e.g.
580 Isometric, 2025; Rainbow, 2025). Our results show that both, mineral weathering and biochar
581 leaching, release cations and increase soil alkalinity, thereby contributing to an IC-sink and
582 interfering with standard ERW MRV protocols where soil alkalinity is considered to remain
583 from geogenic sources only.

584

585 4.3 Chemical fluxes in the soil

586 4.3.1 Pure amendments

587 Carbonate minerals show generally higher weathering rates than silicates (Lasaga and Berner,
588 1998), which is reflected in our data where Ca²⁺ from limestone and industrial materials
589 exhibit the highest fluxes (up to 20.8 kg t⁻¹, Figure 2, supplementary data D7). For peridotite,
590 the IC-sink is mainly driven by Mg²⁺ release from the weathering of olivine, comprising 63.3%
591 of its composition (supplementary data D2). In basanite, Na⁺ dominates the IC-Sink, likely
592 originating from rapidly weathering Na-rich minerals such as leucite, nepheline, and
593 interstitial glass (Dupla et al., 2025). High DSi fluxes in peridotite and basanite reflect
594 weathering of silicate minerals such as olivine and nepheline, while elevated DSi in concrete
595 likely derives from weathering of calcium silicate hydrates, the dominant binding phase in
596 cementitious materials (Multer Hopkins et al., 2024). Biochar shows a small IC-sink (23 kg CO₂
597 t⁻¹), driven primarily by fast leaching of major cations within the first few months which was
598 also observed in other studies (Ding et al., 2010; Meyer zu Drewer et al., 2025). By far the

599 largest contribution to the IC-Sink of biochar comes from K^+ , a common pattern observed
600 especially for biochar based on straw biomass, showing immediate release of K^+ (Ippolito et
601 al., 2020; Meyer zu Drewer et al., 2025).

602 As fluxes from the control soil are subtracted from all amendments, negative fluxes in the
603 leachate indicate a net retention of certain elements. Retention of Ca^{2+} in silicate amendments
604 coincides with strong Mg^{2+} , Na^+ , and DSi release (Figure 2, supplementary data D7), suggesting
605 that a high release of Mg^{2+} could support the formation of Ca-Mg clay minerals (e.g., kaolinite,
606 montmorillonite) and possibly calcite acting as a Ca^{2+} sink. The suggested calcite formation
607 coincides with a higher IC content measured in post-experiment soil analysis for peridotite
608 amendments, which is however not evident in basanite amended soil (supplementary data
609 D10). Other soil columns show a net retention of Mg^{2+} , K^+ and DSi with steel slag, and DSi
610 retention in limestone amendments probably indicating illite and vermiculite formation (Hong
611 et al., 2014; Wilson, 1999). The retention of DSi in the pure biochar amendments may be
612 explained by the adsorption of silicic acid by low-silicon biochar (Wang et al., 2018).

613 The impact of ERW on SOC dynamics has recently gained attention due to likely increased soil
614 respiration evoked from an upward shift of soil pH, higher plant productivity and microbial
615 activity (Anthony et al., 2025; Buss et al., 2024; Fang et al., 2023). While we did not measure
616 soil CO_2 efflux, we assessed DOC fluxes, which are linked to rapid soil pH shifts (Gao et al.,
617 2025) and may provide an indicator of soil carbon losses, as DOC represents a mobile and
618 reactive pool sourced from soil organic matter decomposition (Camino-Serrano et al., 2016;
619 Kalbitz et al., 2000). Only amendments with concrete and limestone, which mostly contain
620 carbonate minerals, show net DOC retention likely related to the stabilization mechanisms of
621 Ca^{2+} on SOC (Rowley et al., 2018; Setia et al., 2014), while silicates, steel slag, and biochar
622 result in DOC release (Figure 2). Assuming a carbon use efficiency of 70%, meaning that 70%
623 of the DOC found in the leachate water will be respired and converted to inorganic CO_2 in the
624 long run (Sinsabaugh et al., 2013), DOC loss from steel slag would reduce its IC-sink by 85%,
625 down to $4.3 \text{ kg } CO_2 \text{ t}^{-1}$. Although increases in soil respiration from ERW have been attributed
626 to pH shifts and enhanced microbial activity (Dupla et al., 2024; Su et al., 2025), the highest
627 delta pH values in our experiment, observed for peridotite, steel slag, and concrete, lead to
628 divergent DOC responses (supplementary information S11 and S12). This suggests that DOC
629 leaching due to increased soil respiration might be more complex than suggested and the

630 composition of the dissolving minerals responsible for the pH increase may play an important
631 role as well.

632 While biochar commonly increases CO₂ efflux through decomposition of its labile fraction
633 (Ansari et al., under review; Kammann et al., 2012; Te Pas et al., 2026; Wang et al., 2016,
634 2014), Chiaravalotti et al. (2025) do not find direct evidence of ERW-induced CO₂ efflux, and
635 DOC dynamics appear more closely tied to soil-specific SOC processes and the Birch effect, the
636 rapid pulse of microbial activity and carbon release that occurs when dry soil is rewetted
637 (Jarvis et al., 2007), rather than to pH alone. Our study confirms the strong impact of the Birch
638 effect as DOC leaching is concentrated in the first year, with more stable flux patterns in
639 basanite, concrete, and limestone treatments during the second year (supplementary
640 information S11, supplementary data D11). Other studies highlight that ERW can enhance SOC
641 sequestration through MAOM formation exceeding the IC-Sink (Xu et al., 2024), promote
642 IC-to-SOC transformation via (hydr)oxides (Niron et al., 2024), and stabilize existing SOC (Boito
643 et al., 2025; Buss et al., 2024; Steinwider et al., 2025), while no effect on any soil carbon pools
644 is also evident (Maxbauer et al., 2026).

645 In our study, DOC responses are not directly linked to high Ca²⁺ fluxes as both retention and
646 leaching occur. For Mg²⁺ from limestone and industrial materials, there seems to be a reverse
647 connection to DOC leaching, where the Mg²⁺ loss from concrete and limestone is associated
648 with DOC retention and the Mg²⁺ retention from steel slag is associated with DOC leaching.
649 This may point towards DOC retention being linked to Mg²⁺ via sorption (Setia et al., 2014)
650 and the Mg²⁺ release from dissolution of 2:1 silicate layer minerals. Slightly elevated SOC
651 contents (up to 0.3% above the control, supplementary data D10) across most amendments
652 likely reflect formation of aluminosilicates, (hydr)oxides, and crystalline minerals, which
653 enhance organo-mineral associations (Liu et al., 2023; Rowley et al., 2018) and may explain a
654 reduced C_{org} loss during the experiment. These patterns do not apply to silicate amendments
655 or biochar. It remains undefined if DOC retention and avoided respiration to inorganic CO₂
656 presents an additional contribution to the total C-Sink. If attributed to the total C-Sink, DOC
657 retention of concrete and limestone amendments could add up to 44% to the IC-Sink and play
658 a major role in SOC build-up for soils.

659 Trace metals remain a concern for ERW, particularly for Ni and Cr released from olivine-rich
660 peridotite (Rijnders et al., 2025). Trace metal concentrations in the leachate peak early during
661 the experiment in week 9, likely due to initial high weathering rates overprinting pH-controlled

662 immobilization (Bang and Hesterberg, 2004; Te Pas et al., 2023). When subtracting trace metal
663 fluxes from the control soil, concentrations exceeding German Drinking Water Ordinance
664 thresholds occur for Ni in peridotite and steel slag and for Pb in biochar (supplementary
665 information S7). The latter suggests that that concerns for trace metals must also be
666 considered in biomass-based CDR and background levels of trace metals in the soil may
667 interfere with monitoring following environmental guidelines. Compared with Rijnders et al.
668 (2025) our results from pure basanite are similar for Cd, Ni and Pb, while leached trace metals
669 from concrete and steel slag weathering were much lower due to lower application rates and
670 probably different material compositions. Similar trace metal concentration trends are
671 reported in other studies for steel slag, basanite, and peridotite (Amann et al., 2020;
672 Steinwider et al., 2026).

673

674 4.3.2 Co-application of minerals and biochar

675 In co-applications, IC-sinks of silicate minerals and concrete are generally elevated, consistent
676 with synergistic increases in the geogenic IC-sink (chapter 4.2.3, Table 6). Ca^{2+} fluxes decrease
677 in both concrete and steel slag co-applications likely indicating the adsorption on charged
678 biochar surfaces. A delayed DSi flux due to adsorption to biochar (Wang et al., 2018) may
679 contribute to secondary mineral formation and reduce the IC-Sink mainly impacting co-
680 applications with concrete and silicate amendments that show large DSi fluxes in general,
681 while this effect hardly occurs for the low DSi release of steel slag (Figure 2). For co-
682 applications with silicates, we observe a lower retention of Ca^{2+} in the soil leading to generally
683 higher IC-Sink and geogenic IC-Sink (Table 6Table 6: The C-Sink potentials and actual C-Sinks
684 from the experiment of all RE-biochars, co-applications and pure amendments are reported
685 as the C-Sink, the inorganic carbon sink (IC-Sink) and the pyrogenic carbon sink (PyC-Sink). The
686 deviation of the measured from the expected C-Sinks and IC-Sinks is expressed as percentage.
687 The deviation of the measured from expected geogenic IC-Sink refers to the IC-Sink solely
688 occurring from mineral weathering (calculated after equations 9-12, supplementary
689 information S6).), while fluxes of K^{+} are mainly contributed by biochar alone.

690 In general, the co-application with biochar has a remarkable effect on DOC leaching (Figure 2,
691 supplements S11). DOC leaching with peridotite, basanite and steel slag is disproportionately
692 reduced compared to expected values and the DOC retention from concrete is not fully
693 counterbalanced by the biochar DOC leaching. These results highlight the importance of

694 organo-mineral interactions in reducing SOC losses and likely promoting MAOM formation
695 (Buss et al., 2024, 2023; Xu et al., 2024). Except for steel slag, the combined CO₂ drawdown
696 remaining from the IC-Sink and DOC retention is higher for the co-applications than for their
697 corresponding single application. The addition of biochar can be seen as an effective measure
698 to counterbalance SOC loss under ERW as already shown in modelling studies (Maslouski et
699 al., 2025). However, trace metal leaching from co-applications of biochar with peridotite and
700 steel slag exceeds net nickel concentrations of the German Drinking Water Ordinance.
701 Co-applications with silicate minerals also exceed lead concentrations, which is mainly
702 attributed to the high lead leaching from biochar, while the leaching of lead from industrial
703 materials is reduced. We assume that high Ca²⁺ fluxes may support the precipitation of PbCO₃
704 in co-precipitation with CaCO₃ (Saleh et al., 2026). Nonetheless, 60% of the co-applications
705 exhibited net trace metal retention (Table 4), demonstrating that this approach still provides
706 a mitigating effect despite these critical cases.

707

708 4.3.3 Co-pyrolysis of minerals and biomass

709 Chemical fluxes RE-biochars produced from dry-mixed and wet-impregnated feedstocks show
710 similar patterns (Figure 2). RE-biochars with concrete, steel slag, and basanite largely follow
711 flux behaviour observed in co-applications. Given their higher mineral content (62.1–67.4
712 wt%), geogenic IC-Sinks are expected to be higher than in co-applications. However, for
713 industrial materials, geogenic IC-sinks are 25–63% below their expected values, indicating
714 suppressed mineral weathering (Table 6). This likely results from partial encapsulation of
715 minerals within the biochar matrix during pyrolysis (Meyer zu Drewer et al., 2025) or a
716 reduction of the mineral surface area from pellet compaction. Another reason could be the
717 impact of pyrolysis temperature on the properties of the carbonate minerals within the
718 industrial materials. Although not detected in the XRD measurements, hydrocarbonates may
719 be present in the non-heated minerals as amorphous minerals (supplementary data D2).
720 When heated to 650 °C, hydrocarbonates undergo complete decomposition, resulting in lower
721 weathering rates (Coenen et al., 2016). In RE-biochars, the basanite K⁺ fluxes mainly stem from
722 biochar (Figure 2, supplementary data D7). The K⁺ fluxes are lower proportional to the biochar
723 content and may suggest a stabilizing effect from co-pyrolysis. The fluxes of all four major
724 cations are generally higher in the basanite RE-biochar with wet-impregnation, suggesting
725 benefits from suspension of the basanite powder.

726 In peridotite RE-biochars, Mg^{2+} and DSi release is strongly enhanced (Figure 2). Given that
727 peridotite contains 19.6% serpentine, pyrolysis likely induced thermal activation, consistent
728 with transformations into metaserpentine and forsterite (Du Breuil et al., 2019). Mg^{2+} leaching
729 increased by 170-175% and remained elevated (2.8×) through week 75, demonstrating
730 long-lasting activation effects by co-pyrolysis. Similar long-term responses have been
731 observed in other thermal activation studies with serpentine-rich rocks (Vorrath et al., in
732 prep.). Although the IC-sink_{pot} of peridotite does not change, accelerated weathering may
733 reduce the time lag before alkalinity becomes detectable in high-CEC soils (Kanzaki et al.,
734 2025). Despite increased DOC leaching from peridotite RE-biochars, the combined CO_2
735 drawdown from the IC-sink and DOC exceeds that of unheated peridotite by a factor of three.

736 Trace metal concentrations from all RE-biochars exceed Pb thresholds of the German Drinking
737 Water Ordinance, and steel slag RE-biochars show elevated Cd, Ni, and Pb, likely due to
738 breakdown of metal-bearing phases during pyrolysis. In contrast, peridotite RE-biochars
739 exhibit lower Ni leaching than untreated peridotite (Table 4, supplementary information S7),
740 increasing its potential application by enhanced trace metal retention for the mineral with the
741 highest risk of nickel contamination in this study.

742

743 4.4 Distribution pathways of released cations

744 Our accounting of cations in the exchangeable fraction of post-experiment soils shows that
745 cation concentrations in the leachate water are 3 to 54 times higher (Table 5). For nearly all
746 amendments, the exchangeable fraction represents only a small proportion of total cation
747 release of maximum 2.1% of the input material. This pattern likely reflects the low CEC and
748 low TOC of the sandy soil, as well as the absence of plants or soil fauna. In contrast, pot
749 experiments with soils of higher CEC show the opposite trend, where most cations are
750 retained in exchangeable fractions, carbonates, (hydr)oxides, or SOM-associated pools, with
751 little or no leaching observed (Boito et al., 2025; Niron et al., 2024; Steinwidder et al., 2026;
752 Te Pas et al., 2026; Vienne et al., 2026b, 2024). This supports the view of Bijma et al. (2026)
753 that robust CDR accounting requires tracking cations across all soil pools, not only in the
754 leachate.

755 Both relative and absolute cation values (Table 5, supplementary data D9) reveal higher
756 proportions of divalent cations (Ca^{2+} , Mg^{2+}) in the exchangeable fraction compared to
757 monovalent cations (K^+ , Na^+), except for Ca^{2+} with all peridotite amendments and pure

758 biochar. Ca^{2+} retention in basanite amendments, indicated by negative values in the leachate
759 water or positive values in the exchangeable fraction, shows that divalent cations first pass
760 through the exchangeable pool before contributing to the IC-sink in the leachate. For
761 peridotite amendments, negative values in both exchangeable and leachate fraction point
762 toward redistribution of Ca^{2+} into other soil pools. Exchangeable Ca^{2+} saturation after the
763 experiment is highest in soils receiving carbonate amendments (0.9 mmol for concrete and
764 limestone) and near zero to negative for silicates (-0.9 mmol for peridotite), consistent with
765 higher Ca^{2+} fluxes as seen in other studies (Hammes et al., 2025). Similar increases in Ca^{2+}
766 saturation during steel slag weathering were also observed by Maxbauer et al. (2026),
767 supporting a proportional relationship between Ca^{2+} saturation and Ca^{2+} release.

768 Although other soil cation pools were not measured, several interactions likely may have
769 influenced Ca^{2+} and Mg^{2+} mobility. Many studies suggest that part of the released cations
770 becomes incorporated into secondary minerals (Dietzen and Rosing, 2023; Hammes et al.,
771 2025; Niron et al., 2024; Steinwider et al., 2026; Te Pas et al., 2026, 2025), and that secondary
772 precipitation may occur even from undersaturated solutions (Ruiz-Agudo et al., 2012).
773 Fast-weathering minerals tend to produce more secondary precipitates, while slowly
774 weathering phases reduce cation incorporation, potentially enhancing CDR by minimizing
775 precipitation losses (Steinwider et al., 2026). In our experiment, only small decreases in
776 inorganic carbon were detected (supplementary data D10), making significant carbonate
777 precipitation unlikely. Amorphous and crystalline phases, including aluminosilicate clays and
778 (hydr)oxides, may serve as sinks for Ca^{2+} and Mg^{2+} , consistent with evidence of Ca^{2+} - and
779 Mg^{2+} -bearing secondary minerals such as kaolinite and 2:1 layer silicates (Steinwider et al.,
780 2026; Te Pas et al., 2026). Interactions of Ca^{2+} and Mg^{2+} with soil organic matter may also
781 contribute to MAOM formation (Buss et al., 2023; Vienne et al., 2026a), potentially supported
782 by iron (hydr)oxide formation, which is known to stabilize SOC over the long term (Kleber et
783 al., 2015; Te Pas et al., 2026). Although SOC stocks increased slightly in most amendments,
784 these results must be interpreted with caution, as fine biochar particles may have contributed
785 to measured SOC despite careful sampling.

786 Monovalent cations (K^+ , Na^+) show higher variability in both exchangeable and leachate
787 fractions, sometimes exceeding their input amounts in treatments with concrete, steel slag,
788 peridotite, and biochar. Na^+ may originate from dissolution of in-situ feldspar and feldspathoid
789 minerals or from exchange with other cations due to preferential adsorption order (Tan,

790 2010), resulting in additional export. Na^+ also serves as a clear indicator of basanite
791 weathering (Dupla et al., 2025), and is mostly exported in the leachate. Elevated K^+ fluxes likely
792 reflect the release of soil inherent K^+ due to cation exchange processes as well. In agricultural
793 settings, plants could access additional K^+ from the soil beyond amendment inputs (Swoboda
794 et al., 2022), though this effect is absent in our plant-free setup.

795 Overall, all amendments show net release of major cations, except for Ca^{2+} and Na^+ in
796 peridotite and Ca^{2+} for basanite amendments. Because we did not measure all soil cation pools
797 (e.g., mineral-associated organic matter, oxide-bound pools), precise weathering
798 quantification is not possible. However, the combined cation release from exchangeable
799 fractions and leachate provides a conservative lower-bound estimate of weathering intensity
800 and exported alkalinity, especially given the soil's low clay and carbonate content. Based on
801 this combined accounting, dissolution over 75 weeks is at least 6.8% for concrete, 5.8% for
802 steel slag, and lower for limestone (4.0%), basanite (4.1%), and peridotite (1.4%)
803 (supplementary data D9).

804

805 5 Conclusion

806 Our study demonstrates that mineral-biochar interactions in soil systems produce distinct and
807 material-specific impacts on C_{org} conversion, mineral weathering, and the formation of both
808 inorganic and organic C-sinks. Co-pyrolysis can enhance carbon retention in biochar,
809 particularly with wet-impregnation of Mg^{2+} ions, but often suppresses carbonate weathering,
810 thereby reducing the geogenic IC-sink. In contrast, co-application of minerals and biochar
811 consistently improves weathering conditions, enhances geogenic IC-sinks for most minerals,
812 and reduces DOC losses, making it an effective and practical strategy for combined CDR
813 approaches under the sandy soil conditions tested here.

814 Among pure mineral amendments, concrete and limestone facilitate DOC retention and
815 achieve moderate IC-sink efficiencies, whereas silicates such as basanite and peridotite
816 contribute more modestly but steadily to long-term alkalinity production. Thermal activation
817 of peridotite through co-pyrolysis remarkably accelerates Mg^{2+} release and inhibits Ni release,
818 highlighting the potential of heat-induced mineral transformations to shorten weathering
819 time lags. However, the benefits of accelerated dissolution must be weighed against increased

820 trace metal mobility and reduced C-sink performance in RE-biochars derived from industrial
821 materials.

822 The distribution of released cations shows that in coarse-textured, low-CEC soils, most cations
823 are exported through leaching rather than retained in exchangeable fractions, allowing
824 leachate fluxes to serve as conservative lower-bound estimates of weathering. Secondary
825 mineral formation likely accounts for part of the missing cation mass balance, underscoring
826 the need for more comprehensive measurements of mineral-associated organic matter,
827 (hydr)oxide pools, and amorphous phases in future experiments.

828 Overall, our findings indicate that co-application of mineral powders and biochar offers the
829 best balance between C-sink formation, weathering enhancement, trace-metal safety, and
830 operational feasibility. RE-biochars may provide targeted benefits, such as improved carbon
831 stability, increased C_{org} conversion into biochar or accelerated silicate dissolution, but they do
832 not consistently outperform simpler deployment strategies. For field implementation,
833 site-specific soil properties, mineral composition, regulatory thresholds for trace metals, and
834 broader logistical considerations must be carefully integrated into amendment selections and
835 MRV frameworks. Our results highlight the need for long-term field studies and multi-pool
836 carbon accounting to fully capture mineral-organic interactions and optimise combined
837 ERW-biochar strategies for durable carbon removal.

838

839 **Acknowledgements**

840 We warmly want to thank our lab technicians Peggy Bartsch and Tom Jäppinen and our
841 student assistant Irmak Gök. We also thank Peter Stutz and Stefan Jung from the University of
842 Hamburg for XRF measurements, Sebastian Lindhorst from the University of Hamburg for
843 grain size distribution measurements, José Maria de la Rosa from the Institute of Natural
844 Resources and Agrobiology of Sevilla for TGA measurements, William Meredith from the
845 University of Nottingham for hydrolysis analyses, the team from the Element Analysis,
846 Chemistry Department, University Hamburg for the trace metal analyses, and Sören
847 Beckmann for logistical support at the Geomatikum, University of Hamburg.

848 We also like to thank for the trust and the support from Caspar von Ziegner, Esther Jäckel,
849 Jens Heberling and Lars Macketanz from Novocarbo, Michael Dohlen from Thyssenkrupp AG,

850 Maurice Bryson from Silicate Carbon Limited and Andrew Simeonidis from Sibelco. We also
851 thank Nikolas Hagemann from the Ithaka Institute for Carbon Strategies, Germany.

852

853 **Author contributions**

854 MEV conceptualized and coordinated the research project and acquired the funding, designed
855 the study, prepared visualizations and wrote the original manuscript. MEV, JMD, CA, LS, LF,
856 SN, IN performed the experiments. MEV and JMD analysed the data. MS and TS assisted with
857 the pellet press, DE provided AAS measurements for trace metals. JH supported with the
858 institutional framework. All authors contributed to the discussion and manuscript writing and
859 provided valuable input.

860

861 **Funding Sources**

862 The project proudly received funding as “The Rockchar Project” from the Klaus Tschira Boost
863 Fund, a joint initiative of GSO – Guidance, Skills & Opportunities for Researchers e.V. and the
864 Klaus Tschira Stiftung.

865

866 **References**

- 867 Amann, T., Hartmann, J., 2019. Ideas and perspectives: Synergies from co-deployment of
868 negative emission technologies. *Biogeosciences* 16, 2949–2960.
869 <https://doi.org/10.5194/bg-16-2949-2019>
- 870 Amann, T., Hartmann, J., Hellmann, R., Pedrosa, E.T., Malik, A., 2022. Enhanced weathering
871 potentials—the role of in situ CO₂ and grain size distribution. *Front. Clim.* 4, 929268.
872 <https://doi.org/10.3389/fclim.2022.929268>
- 873 Amann, T., Hartmann, J., Struyf, E., De Oliveira Garcia, W., Fischer, E.K., Janssens, I., Meire, P.,
874 Schoelynck, J., 2020. Enhanced Weathering and related element fluxes – a cropland
875 mesocosm approach. *Biogeosciences* 17, 103–119. <https://doi.org/10.5194/bg-17-103-2020>
- 877 Ansari, M., Lübeck, A., Meyer zu Drewer, J., Hagemann, N., Eschenbach, A., Becker, J.N., under
878 review. Rock-enhanced biochar has similar priming effect as pure biochar application,
879 but improves short-term carbon stabilization in agricultural soils. *Biology and Fertility*
880 *of Soils*.
- 881 Ansari, M., Stock, S., Dippold, M.A., Hamburger, S.E., Kammann, C.I., Meyer Zu Drewer, J.,
882 Hagemann, N., Eschenbach, A., Becker, J.N., 2026. Biochar dominated the combined
883 effect of silicate rock powder and biochar application on extracellular enzyme kinetics
884 and nutrient dynamics in a sandy soil. *Soil and Tillage Research* 262, 107234.
885 <https://doi.org/10.1016/j.still.2026.107234>

- 886 Anthony, T.L., Jones, A.R., Silver, W.L., 2025. Supplementing Enhanced Weathering With
887 Organic Amendments Accelerates the Net Climate Benefit of Soil Amendments in
888 Rangeland Soils. *AGU Advances* 6, e2024AV001480.
889 <https://doi.org/10.1029/2024AV001480>
- 890 Azzi, E.S., Li, H., Cederlund, H., Karlton, E., Sundberg, C., 2024. Modelling biochar long-term
891 carbon storage in soil with harmonized analysis of decomposition data. *Geoderma* 441,
892 116761. <https://doi.org/10.1016/j.geoderma.2023.116761>
- 893 Babiker, M., Berndes, G., Blok, K., Cohen, B., Cowie, A., Geden, O., Ginzburg, V., Leip, A., Smith,
894 P., Sugiyama, M., Yamba, F., 2022. Cross-sectoral perspectives, in: Shukla, P.R., Skea,
895 J., Slade, R., Al Khourdajie, A., van Diemen, R., McCollum, D., Pathak, M., Some, S.,
896 Vyas, P., Fradera, R., Belkacemi, M., Hasija, A., Lisboa, G., Luz, S., Malley, J. (Eds.),
897 Climate Change 2022: Mitigation of Climate Change. Contribution of Working Group III
898 to the Sixth Assessment Report of the Intergovernmental Panel on Climate Change.
899 Cambridge University Press, Cambridge, UK and New York, NY, USA, pp. 1245–1354.
900 <https://doi.org/10.1017/9781009157926.014>
- 901 Bang, J., Hesterberg, D., 2004. Dissolution of trace element contaminants from two coastal
902 plain soils as affected by pH. *J Environ Qual* 33, 891–901.
903 <https://doi.org/10.2134/jeq2004.0891>
- 904 Beerling, D.J., Leake, J.R., Long, S.P., Scholes, J.D., Ton, J., Nelson, P.N., Bird, M., Kantzas, E.,
905 Taylor, L.L., Sarkar, B., Kelland, M., DeLucia, E., Kantola, I., Müller, C., Rau, G., Hansen,
906 J., 2018. Farming with crops and rocks to address global climate, food and soil security.
907 *Nature Plants* 4, 138–147. <https://doi.org/10.1038/s41477-018-0108-y>
- 908 Bijma, J., Hagens, M., Hammes, J.S., Planavsky, N., Pogge Von Strandmann, P.A.E.,
909 Reershemius, T., Reinhard, C.T., Renforth, P., Suhrhoff, T.J., Vicca, S., Vienne, A., Wolf-
910 Gladrow, D., 2026. Reviews and syntheses: Carbon vs. cation based MRV of Enhanced
911 Rock Weathering and the issue of soil organic carbon. *Biogeosciences* 23, 53–75.
912 <https://doi.org/10.5194/bg-23-53-2026>
- 913 Boito, L., Steinwider, L., Rijnders, J., Berwouts, J., Janse, S., Niron, H., Roussard, J., Vienne, A.,
914 Vicca, S., 2025. Enhanced Rock Weathering Altered Soil Organic Carbon Fluxes in a
915 Plant Trial. *Global Change Biology* 31, e70373. <https://doi.org/10.1111/gcb.70373>
- 916 Borchard, N., Schirrmann, M., Cayuela, M.L., Kammann, C., Wrage-Mönnig, N., Estavillo, J.M.,
917 Fuertes-Mendizábal, T., Sigua, G., Spokas, K., Ippolito, J.A., Novak, J., 2019. Biochar,
918 soil and land-use interactions that reduce nitrate leaching and N₂O emissions: A meta-
919 analysis. *Science of The Total Environment* 651, 2354–2364.
920 <https://doi.org/10.1016/j.scitotenv.2018.10.060>
- 921 Buckingham, F.L., Henderson, G.M., 2024. The enhanced weathering potential of a range of
922 silicate and carbonate additions in a UK agricultural soil. *Science of The Total*
923 *Environment* 907, 167701. <https://doi.org/10.1016/j.scitotenv.2023.167701>
- 924 Buss, W., Hasemer, H., Ferguson, S., Borevitz, J., 2023. Stabilisation of soil organic matter with
925 rock dust partially counteracted by plants. *Global Change Biology* 30, e17052.
926 <https://doi.org/10.1111/gcb.17052>
- 927 Buss, W., Hasemer, H., Sokol, N.W., Rohling, E.J., Borevitz, J., 2024. Applying minerals to soil
928 to draw down atmospheric carbon dioxide through synergistic organic and inorganic
929 pathways. *Commun Earth Environ* 5, 602. [https://doi.org/10.1038/s43247-024-01771-](https://doi.org/10.1038/s43247-024-01771-3)
930 [3](https://doi.org/10.1038/s43247-024-01771-3)
- 931 Buss, W., Jansson, S., Wurzer, C., Mašek, O., 2019. Synergies between BECCS and Biochar—
932 Maximizing Carbon Sequestration Potential by Recycling Wood Ash. *ACS Sustainable*
933 *Chem. Eng.* 7, 4204–4209. <https://doi.org/10.1021/acssuschemeng.8b05871>

934 Buss, W., Wurzer, C., Manning, D.A.C., Rohling, E.J., Borevitz, J., Mašek, O., 2022. Mineral-
935 enriched biochar delivers enhanced nutrient recovery and carbon dioxide removal.
936 *Commun Earth Environ* 3, 67. <https://doi.org/10.1038/s43247-022-00394-w>

937 Camino-Serrano, M., Graf Pannatier, E., Vicca, S., Luysaert, S., Jonard, M., Ciais, P., Guenet,
938 B., Gielen, B., Peñuelas, J., Sardans, J., Waldner, P., Etzold, S., Cecchini, G., Clarke, N.,
939 Galić, Z., Gandois, L., Hansen, K., Johnson, J., Klinck, U., Lachmanová, Z., Lindroos, A.-
940 J., Meesenburg, H., Nieminen, T.M., Sanders, T.G.M., Sawicka, K., Seidling, W.,
941 Thimonier, A., Vanguelova, E., Verstraeten, A., Vesterdal, L., Janssens, I.A., 2016.
942 Trends in soil solution dissolved organic carbon (DOC) concentrations across European
943 forests. *Biogeosciences* 13, 5567–5585. <https://doi.org/10.5194/bg-13-5567-2016>

944 Chiaravalloti, I., Zhang, S., Planavsky, N., 2025. Assessing CO₂ fluxes during enhanced
945 weathering from soils through a mesocosm lens. *CDRXIV*.

946 Cipolla, G., Calabrese, S., Porporato, A., Noto, L.V., 2022. Effects of precipitation seasonality,
947 irrigation, vegetation cycle and soil type on enhanced weathering – modeling of
948 cropland case studies across four sites. *Biogeosciences* 19, 3877–3896.
949 <https://doi.org/10.5194/bg-19-3877-2022>

950 Coenen, K., Gallucci, F., Cobden, P., van Dijk, E., Hensen, E., van Sint Annaland, M., 2016.
951 Chemisorption working capacity and kinetics of CO₂ and H₂O of hydrotalcite-based
952 adsorbents for sorption-enhanced water-gas-shift applications. *Chemical Engineering*
953 *Journal* 293, 9–23. <https://doi.org/10.1016/j.cej.2016.02.050>

954 Cornelissen, G., Briels, N., Bucheli, T.D., Estoppey, N., Gredelj, A., Hagemann, N., Lerch, S., Lotz,
955 S., Rasse, D., Schmidt, H.-P., Sørmo, E., Arp, H.P.H., 2025. A Virtuous Cycle of
956 Phytoremediation, Pyrolysis, and Biochar Applications toward Safe PFAS Levels in Soil,
957 Feed, and Food. *J. Agric. Food Chem.* 73, 3283–3285.
958 <https://doi.org/10.1021/acs.jafc.5c00651>

959 Deng, H., Sonnenthal, E., Arora, B., Breunig, H., Brodie, E., Kleber, M., Spycher, N., Nico, P.,
960 2023. The environmental controls on efficiency of enhanced rock weathering in soils.
961 *Sci Rep* 13, 9765. <https://doi.org/10.1038/s41598-023-36113-4>

962 Dietzen, C., Rosing, M.T., 2023. Quantification of CO₂ uptake by enhanced weathering of
963 silicate minerals applied to acidic soils. *International Journal of Greenhouse Gas*
964 *Control* 125, 103872. <https://doi.org/10.1016/j.ijggc.2023.103872>

965 Ding, Y., Liu, Y.-X., Wu, W.-X., Shi, D.-Z., Yang, M., Zhong, Z.-K., 2010. Evaluation of Biochar
966 Effects on Nitrogen Retention and Leaching in Multi-Layered Soil Columns. *Water Air*
967 *Soil Pollut* 213, 47–55. <https://doi.org/10.1007/s11270-010-0366-4>

968 Du Breuil, C., César-Pasquier, L., Dipple, G., Blais, J.-F., Iliuta, M., Mercier, G., 2019.
969 Mineralogical Transformations of Heated Serpentine and Their Impact on Dissolution
970 during Aqueous-Phase Mineral Carbonation Reaction in Flue Gas Conditions. *Minerals*
971 9, 680. <https://doi.org/10.3390/min9110680>

972 Dupla, X., Bertagni, M.B., Grand, S., 2025. Three Years of Field Trials Indicate a Sustained
973 Enhanced Rock Weathering Signal with Limited CO₂ Removal. *Environ. Sci. Technol.*
974 59, 25751–25764. <https://doi.org/10.1021/acs.est.5c09820>

975 Dupla, X., Claustre, R., Bonvin, E., Graf, I., Le Bayon, R.-C., Grand, S., 2024. Let the dust settle:
976 Impact of enhanced rock weathering on soil biological, physical, and geochemical
977 fertility. *Science of The Total Environment* 954, 176297.
978 <https://doi.org/10.1016/j.scitotenv.2024.176297>

979 EBC, 2024. Guidelines for a Sustainable Production of Biochar (No. Version 10.4G). Ithaca
980 Institute, Arbaz, Switzerland.

981 Fang, Q., Lu, A., Hong, H., Kuzyakov, Y., Algeo, T.J., Zhao, L., Olshansky, Y., Moravec, B.,
982 Barrientes, D.M., Chorover, J., 2023. Mineral weathering is linked to microbial priming
983 in the critical zone. *Nat Commun* 14, 345. [https://doi.org/10.1038/s41467-022-35671-](https://doi.org/10.1038/s41467-022-35671-x)
984 [x](https://doi.org/10.1038/s41467-022-35671-x)

985 Gao, H., Weng, L., Comans, R.N.J., Koopmans, G.F., 2025. Dual-Domain Regulation of Dissolved
986 Organic Matter Release in Soil: The Role of pH and Calcium. *ACS Earth Space Chem.* 9,
987 1377–1391. <https://doi.org/10.1021/acsearthspacechem.4c00377>

988 Grafmüller, J., Böhm, A., Zhuang, Y., Spahr, S., Müller, P., Otto, T.N., Bucheli, T.D., Leifeld, J.,
989 Giger, R., Tobler, M., Schmidt, H.-P., Dahmen, N., Hagemann, N., 2022. Wood Ash as
990 an Additive in Biomass Pyrolysis: Effects on Biochar Yield, Properties, and Agricultural
991 Performance. *ACS Sustainable Chem. Eng.* 10, 2720–2729.
992 <https://doi.org/10.1021/acssuschemeng.1c07694>

993 Hagemann, N., Schmidt, H.-P., Bucheli, T.D., Grafmüller, J., Vosswinkel, S., Herdegen, V.,
994 Meredith, W., Uguna, C.N., Snape, C.E., 2025. Proxies for use in biochar decay models:
995 Hydropyrolysis, electric conductivity, and H/Corg molar ratio. *PLoS One* 20, e0330206.
996 <https://doi.org/10.1371/journal.pone.0330206>

997 Hammes, J.S., Hartmann, J., Barth, J.A.C., Linke, T., Smet, I., Hagens, M., Pogge Von
998 Strandmann, P.A.E., Reershemius, T., Casimiro, B., Vienne, A., Stoeckel, A.A., Steffens,
999 R., Paessler, D., 2025. Soil processes govern alkalinity and cation retention in enhanced
1000 weathering for carbon dioxide removal. [https://doi.org/10.5194/egusphere-2025-](https://doi.org/10.5194/egusphere-2025-5402)
1001 [5402](https://doi.org/10.5194/egusphere-2025-5402)

1002 Han, L., Sun, K., Yang, Y., Xia, X., Li, F., Yang, Z., Xing, B., 2020. Biochar's stability and effect on
1003 the content, composition and turnover of soil organic carbon. *Geoderma* 364, 114184.
1004 <https://doi.org/10.1016/j.geoderma.2020.114184>

1005 Haque, F., Santos, R.M., Chiang, Y.W., 2020. Optimizing Inorganic Carbon Sequestration and
1006 Crop Yield With Wollastonite Soil Amendment in a Microplot Study. *Frontiers in Plant*
1007 *Science* 11.

1008 Hartmann, J., West, A.J., Renforth, P., Köhler, P., De La Rocha, C.L., Wolf-Gladrow, D.A., Dürr,
1009 H.H., Scheffran, J., 2013. Enhanced chemical weathering as a geoengineering strategy
1010 to reduce atmospheric carbon dioxide, supply nutrients, and mitigate ocean
1011 acidification. *Rev. Geophys.* 51, 113–149. <https://doi.org/10.1002/rog.20004>

1012 Heřmanská, M., Voigt, M.J., Marieni, C., Declercq, J., Oelkers, E.H., 2023. A comprehensive and
1013 consistent mineral dissolution rate database: Part II: Secondary silicate minerals.
1014 *Chemical Geology* 636, 121632. <https://doi.org/10.1016/j.chemgeo.2023.121632>

1015 Heřmanská, M., Voigt, M.J., Marieni, C., Declercq, J., Oelkers, E.H., 2022. A comprehensive and
1016 internally consistent mineral dissolution rate database: Part I: Primary silicate minerals
1017 and glasses. *Chemical Geology* 597, 120807.
1018 <https://doi.org/10.1016/j.chemgeo.2022.120807>

1019 Hong, H., Churchman, G.J., Yin, K., Li, R., Li, Z., 2014. Randomly interstratified illite–vermiculite
1020 from weathering of illite in red earth sediments in Xuancheng, southeastern China.
1021 *Geoderma* 214–215, 42–49. <https://doi.org/10.1016/j.geoderma.2013.10.004>

1022 Honvault, N., Tiouchichine, M.-L., Sauze, J., Piel, C., Landais, D., Devidal, S., Gritti, E., Bosch, D.,
1023 Milcu, A., 2024. Additive effects of basalt enhanced weathering and biochar co-
1024 application on carbon sequestration, soil nutrient status and plant performance in a
1025 mesocosm experiment. *Applied Geochemistry* 169, 106054.
1026 <https://doi.org/10.1016/j.apgeochem.2024.106054>

1027 Ippolito, J.A., Cui, L., Kammann, C., Wrage-Mönnig, N., Estavillo, J.M., Fuertes-Mendizabal, T.,
1028 Cayuela, M.L., Sigua, G., Novak, J., Spokas, K., Borchard, N., 2020. Feedstock choice,

1029 pyrolysis temperature and type influence biochar characteristics: a comprehensive
1030 meta-data analysis review. *Biochar* 2, 421–438. [https://doi.org/10.1007/s42773-020-](https://doi.org/10.1007/s42773-020-00067-x)
1031 00067-x

1032 Isometric, 2025. Enhanced Weathering in Agriculture v1.1.
1033 [https://registry.isometric.com/protocol/enhanced-weathering-](https://registry.isometric.com/protocol/enhanced-weathering-agriculture/enhanced-weathering-agriculture/1.1/1.1.2)
1034 agriculture/enhanced-weathering-agriculture/1.1/1.1.2

1035 Janssens, I.A., Roobroeck, D., Sardans, J., Obersteiner, M., Peñuelas, J., Richter, A., Smith, P.,
1036 Verbruggen, E., Vicca, S., 2022. Negative erosion and negative emissions: Combining
1037 multiple land-based carbon dioxide removal techniques to rebuild fertile topsoils and
1038 enhance food production. *Front. Clim.* 4, 928403.
1039 <https://doi.org/10.3389/fclim.2022.928403>

1040 Jiang, Y., Zhou, L., Zhu, Z., Ma, L., Chen, J., Li, Y., 2022. Research on dynamic cracking properties
1041 of cracked rock mass under the effect of thermal treatment. *Theoretical and Applied*
1042 *Fracture Mechanics* 122, 103580. <https://doi.org/10.1016/j.tafmec.2022.103580>

1043 Kalbitz, K., Solinger, S., Park, J.-H., Michalzik, B., Matzner, E., 2000. CONTROLS ON THE
1044 DYNAMICS OF DISSOLVED ORGANIC MATTER IN SOILS: A REVIEW. *Soil Science* 165,
1045 277.

1046 Kammann, C., Ratering, S., Eckhard, C., Müller, C., 2012. Biochar and Hydrochar Effects on
1047 Greenhouse Gas (Carbon Dioxide, Nitrous Oxide, and Methane) Fluxes from Soils.
1048 *Journal of Environmental Quality* 41, 1052–1066.
1049 <https://doi.org/10.2134/jeq2011.0132>

1050 Kantola, I.B., Blanc-Betes, E., Masters, M.D., Chang, E., Marklein, A., Moore, C.E., Von Haden,
1051 A., Bernacchi, C.J., Wolf, A., Epihov, D.Z., Beerling, D.J., DeLucia, E.H., 2023. Improved
1052 net carbon budgets in the US Midwest through direct measured impacts of enhanced
1053 weathering. *Global Change Biology* 29, 7012–7028.
1054 <https://doi.org/10.1111/gcb.16903>

1055 Kanzaki, Y., Planavsky, N.J., Zhang, S., Jordan, J., Suhrhoff, T.J., Reinhard, C.T., 2025. Soil cation
1056 storage is a key control on the carbon removal dynamics of enhanced weathering.
1057 *Environ. Res. Lett.* 20, 074055. <https://doi.org/10.1088/1748-9326/ade0d5>

1058 Karr-Lilienthal, L.K., Grieshop, C.M., Merchen, N.R., Mahan, D.C., Fahey, G.C., 2004. Chemical
1059 Composition and Protein Quality Comparisons of Soybeans and Soybean Meals from
1060 Five Leading Soybean-Producing Countries. *J. Agric. Food Chem.* 52, 6193–6199.
1061 <https://doi.org/10.1021/jf049795+>

1062 Keiluweit, M., Nico, P.S., Johnson, M.G., Kleber, M., 2010. Dynamic Molecular Structure of
1063 Plant Biomass-Derived Black Carbon (Biochar). *Environ. Sci. Technol.* 44, 1247–1253.
1064 <https://doi.org/10.1021/es9031419>

1065 Kelemen, P.B., Matter, J., Streit, E.E., Rudge, J.F., Curry, W.B., Blusztajn, J., 2011. Rates and
1066 Mechanisms of Mineral Carbonation in Peridotite: Natural Processes and Recipes for
1067 Enhanced, in situ CO₂ Capture and Storage. *Annual Review of Earth and Planetary*
1068 *Sciences* 39, 545–576. <https://doi.org/10.1146/annurev-earth-092010-152509>

1069 Kitsopoulos, K.P., 1999. Cation-Exchange Capacity (CEC) of Zeolitic Volcaniclastic Materials:
1070 Applicability of the Ammonium Acetate Saturation (AMAS) Method. *Clays and clay*
1071 *miner.* 47, 688–696. <https://doi.org/10.1346/CCMN.1999.0470602>

1072 Kleber, M., Eusterhues, K., Keiluweit, M., Mikutta, C., Mikutta, R., Nico, P.S., 2015. Mineral–
1073 Organic Associations: Formation, Properties, and Relevance in Soil Environments, in:
1074 *Advances in Agronomy.* Elsevier, pp. 1–140.
1075 <https://doi.org/10.1016/bs.agron.2014.10.005>

1076 Lalitha, M., Parvathy, S., Koyal, A., Hegde, R., Ramamurthy, V., 2026. Impact of Calcium
1077 Carbonate Solubility on Estimating Soil Exchangeable Cations in Calcareous Soils Using
1078 1N Ammonium Acetate Method. *Communications in Soil Science and Plant Analysis*
1079 57, 480–490. <https://doi.org/10.1080/00103624.2026.2617299>

1080 Lasaga, A.C., Berner, R.A., 1998. Fundamental aspects of quantitative models for geochemical
1081 cycles. *Chemical Geology* 145, 161–175. [https://doi.org/10.1016/S0009-
1082 2541\(97\)00142-3](https://doi.org/10.1016/S0009-2541(97)00142-3)

1083 Lehmann, J., Cowie, A., Masiello, C.A., Kammann, C., Woolf, D., Amonette, J.E., Cayuela, M.L.,
1084 Camps-Arbestain, M., Whitman, T., 2021. Biochar in climate change mitigation. *Nat.*
1085 *Geosci.* 14, 883–892. <https://doi.org/10.1038/s41561-021-00852-8>

1086 Li, F., Cao, X., Zhao, L., Wang, J., Ding, Z., 2014. Effects of Mineral Additives on Biochar
1087 Formation: Carbon Retention, Stability, and Properties. *Environ. Sci. Technol.* 48,
1088 11211–11217. <https://doi.org/10.1021/es501885n>

1089 Li, L., Zhang, Y.-J., Novak, A., Yang, Y., Wang, J., 2021. Role of Biochar in Improving Sandy Soil
1090 Water Retention and Resilience to Drought. *Water* 13, 407.
1091 <https://doi.org/10.3390/w13040407>

1092 Liu, D., Li, M., Yu, R., Li, H., Shen, Y., Tian, Q., Bu, H., Huang, C., Tan, W., 2023. Interlayer organic
1093 matter within hydroxy-interlayered clay minerals enhances soil organic carbon stability
1094 under long-term organic fertilization. *Applied Clay Science* 239, 106963.
1095 <https://doi.org/10.1016/j.clay.2023.106963>

1096 Ma, Z., Yang, Y., Wu, Y., Xu, J., Peng, H., Liu, X., Zhang, W., Wang, S., 2019. In-depth comparison
1097 of the physicochemical characteristics of bio-char derived from biomass pseudo
1098 components: Hemicellulose, cellulose, and lignin. *Journal of Analytical and Applied
1099 Pyrolysis* 140, 195–204. <https://doi.org/10.1016/j.jaap.2019.03.015>

1100 Mahanta, B., Singh, T.N., Ranjith, P.G., 2016. Influence of thermal treatment on mode I
1101 fracture toughness of certain Indian rocks. *Engineering Geology* 210, 103–114.
1102 <https://doi.org/10.1016/j.enggeo.2016.06.008>

1103 Mašek, O., Buss, W., Brownsort, P., Rovere, M., Tagliaferro, A., Zhao, L., Cao, X., Xu, G., 2019.
1104 Potassium doping increases biochar carbon sequestration potential by 45%, facilitating
1105 decoupling of carbon sequestration from soil improvement. *Sci Rep* 9, 5514.
1106 <https://doi.org/10.1038/s41598-019-41953-0>

1107 Maslouski, M., Ansari, M., Hamburger, S.E., Meyer Zu Drewer, J., Hagemann, N., Eschenbach,
1108 A., Beer, C., Becker, J.N., Kammann, C.I., Vorrath, M.-E., Porada, P., 2025. Long-term
1109 carbon dioxide removal potential from the application of wood biochar and basanite
1110 rock powder in sandy soil using the LiDELSv2 process-based modeling approach.
1111 *Environ. Res. Lett.* 20, 124032. <https://doi.org/10.1088/1748-9326/ae21f6>

1112 Maxbauer, D.P., Milliken, E., Yaming, J.R., Watson, E., Gregg, R.B., Swanson, L., Sohng, J.,
1113 Sokol, N.W., Planavsky, N.J., 2026. Evidence for carbon dioxide removal via enhanced
1114 rock weathering with steel slag, though not basalt, in a midwestern U.S. field trial.
1115 *Front. Clim.* 7, 1657058. <https://doi.org/10.3389/fclim.2025.1657058>

1116 Mbow, C., Rosenzweig, C., Barioni, L.G., Benton, T.G., Herrero, M., Krishnapillai, M., Liwenga,
1117 E., Pradhan, P., Rivera-Ferre, M.G., Sapkota, T., Tubiello, F.N., Xu, Y., 2022. Food
1118 Security, in: Shukla, P.R., Skea, J., Calvo Buendia, E., Masson-Delmotte, V., Pörtner, H.-
1119 O., Roberts, D.C., Zhai, P., Slade, R., Connors, S.L., van Diemen, R., Ferrat, M., Haughey,
1120 E., Luz, S., Neogi, S., Pathak, M., Petzold, J., Portugal-Pereira, J., Vyas, P., Huntley, E.,
1121 Kissick, K., Belkacemi, M., Malley, J. (Eds.), *Climate Change and Land: IPCC Special
1122 Report on Climate Change, Desertification, Land Degradation, Sustainable Land*

1123 Management, Food Security, and Greenhouse Gas Fluxes in Terrestrial Ecosystems.
1124 Cambridge University Press. <https://doi.org/10.1017/9781009157988>

1125 McDermott, F., Bryson, M., Magee, R., Van Acken, D., 2024. Enhanced weathering for CO₂
1126 removal using carbonate-rich crushed returned concrete; a pilot study from SE Ireland.
1127 Applied Geochemistry 169, 106056.
1128 <https://doi.org/10.1016/j.apgeochem.2024.106056>

1129 Meredith, W., McBeath, A., Ascough, P., Bird, M.I., 2017. Analysis of biochars by
1130 hydropyrolysis (HyPy), in: Singh, B., Camps Arbestain, M., Lehmann, J. (Eds.), . CRC
1131 Press, Clayton.

1132 Meyer zu Drewer, J., Vorrath, M.-E., Amann, T., Hartmann, J., Ansari, M., Cárcamo Perez, M.,
1133 Hagemann, N., submitted. Combining biochar and basanite rock powder enhances
1134 carbon dioxide removal by carbonate alkalinity production. *Frontiers in Climate*.

1135 Meyer zu Drewer, J., Vorrath, M.-E., Amann, T., Hartmann, J., De La Rosa, J.M., Möllmer, J.,
1136 Pérez-Dalí, S.M., Meredith, W., Uguna, C., Snape, C., Kammann, C., Schmidt, H.-P.,
1137 Hagemann, N., 2025. Pyrogenic carbon and carbonating minerals for carbon capture
1138 and storage (PyMiCCS) part I: production, physico-chemical characterization and C-sink
1139 potential. *Front. Clim.* 7. <https://doi.org/10.3389/fclim.2025.1631368>

1140 Multer Hopkins, B., Lal, R., Lyons, W.B., Welch, S.A., 2024. Carbon capture potential and
1141 environmental impact of concrete weathering in soil. *Science of The Total Environment*
1142 957, 177692. <https://doi.org/10.1016/j.scitotenv.2024.177692>

1143 Nabuurs, G.-J., Mrabet, R., Abu Hatab, A., Bustamante, M., Clark, H., Havlík, P., House, J.I.,
1144 Mbow, C., Ninan, K.N., Popp, A., Roe, S., Sohngen, B., Towprayoon, S., 2022.
1145 Agriculture, Forestry and Other Land Uses (AFOLU), in: Shukla, P.R., Skea, J., Slade, R.,
1146 Al Khourdajie, A., van Diemen, R., McCollum, D., Pathak, M., Some, S., Vyas, P., Fradera,
1147 R., Belkacemi, M., Hasija, A., Lisboa, G., Luz, S., Malley, J. (Eds.), *Climate Change 2022:
1148 Mitigation of Climate Change. Contribution of Working Group III to the Sixth
1149 Assessment Report of the Intergovernmental Panel on Climate Change*. Cambridge
1150 University Press, Cambridge, UK and New York, NY, USA, pp. 747–860.
1151 <https://doi.org/10.1017/9781009157926.009>

1152 Nan, H., Mašek, O., Yang, F., Xu, X., Qiu, H., Cao, X., Zhao, L., 2022. Minerals: A missing role for
1153 enhanced biochar carbon sequestration from the thermal conversion of biomass to
1154 the application in soil. *Earth-Science Reviews* 234, 104215.
1155 <https://doi.org/10.1016/j.earscirev.2022.104215>

1156 Nan, H., Zhao, L., Yang, F., Liu, Y., Xiao, Z., Cao, X., Qiu, H., 2020. Different alkaline minerals
1157 interacted with biomass carbon during pyrolysis: Which one improved biochar carbon
1158 sequestration? *Journal of Cleaner Production* 255, 120162.
1159 <https://doi.org/10.1016/j.jclepro.2020.120162>

1160 Nieuwenhuize, J., Maas, Y.E.M., Middelburg, J.J., 1994. Rapid analysis of organic carbon and
1161 nitrogen in particulate materials. *Marine Chemistry* 45, 217–224.
1162 [https://doi.org/10.1016/0304-4203\(94\)90005-1](https://doi.org/10.1016/0304-4203(94)90005-1)

1163 Niron, H., Vienne, A., Frings, P., Poetra, R., Vicca, S., 2024. Exploring the synergy of enhanced
1164 weathering and *Bacillus subtilis*: A promising strategy for sustainable agriculture.
1165 *Global Change Biology* 30, e17511. <https://doi.org/10.1111/gcb.17511>

1166 Oelkers, E.H., Declercq, J., Saldi, G.D., Gislason, S.R., Schott, J., 2018. Olivine dissolution rates:
1167 A critical review. *Chemical Geology* 500, 1–19.
1168 <https://doi.org/10.1016/j.chemgeo.2018.10.008>

1169 Omara, P., Singh, H., Singh, K., Sharma, L., Otim, F., Obia, A., 2023. Short-term effect of field
1170 application of biochar on cation exchange capacity, pH, and electrical conductivity of

1171 sandy and clay loam temperate soils. TIA 3, 0–0. <https://doi.org/10.48130/TIA-2023->
1172 0016

1173 Palansooriya, K.N., Wong, J.T.F., Hashimoto, Y., Huang, L., Rinklebe, J., Chang, S.X., Bolan, N.,
1174 Wang, H., Ok, Y.S., 2019. Response of microbial communities to biochar-amended
1175 soils: a critical review. *Biochar* 1, 3–22. <https://doi.org/10.1007/s42773-019-00009-2>
1176 Parkhurst, D.L., Appelo, C.A.J., 2013. Description of input and examples for PHREEQC version
1177 3—A computer program for speciation, batch-reaction, one-dimensional transport,
1178 and inverse geochemical calculations, in: U.S. Geological Survey Techniques and
1179 Methods. U.S. Geological Survey, Denver, p. 497.

1180 Peng, X., Deng, Y., Peng, Y., Yue, K., 2018. Effects of biochar addition on toxic element
1181 concentrations in plants: A meta-analysis. *Science of The Total Environment* 616–617,
1182 970–977. <https://doi.org/10.1016/j.scitotenv.2017.10.222>

1183 Pignatello, J.J., Uchimiya, M., Abiven, S., 2024. Aging of biochar in soils and its implications, in:
1184 *Biochar for Environmental Management*. Routledge.

1185 Planavsky, N.J., Ahmed, A.A., Suhrhoff, T.J., Reinhard, C.T., 2024. Cation uptake by biochar
1186 reduces carbon removal efficiency.

1187 Rainbow, 2025. Enhanced rock weathering 1.0.
1188 <https://docs.rainbowstandard.io/methodologies/enhanced-rock-weathering>

1189 Renforth, P., 2019. The negative emission potential of alkaline materials. *Nat Commun* 10,
1190 1401. <https://doi.org/10.1038/s41467-019-09475-5>

1191 Rieder, L., Hagens, M., Poetra, R., Vidal, A., Calogiuri, T., Neubeck, A., Singh, A., Corbett, T.,
1192 Niron, H., Vicca, S., Vlaeminck, S.E., Janssens, Iris, Verdonck, T., Janssens, Ivan, Li, X.,
1193 Hammes, J.S., Hartmann, J., 2026. Contribution of dissolved organic carbon to total
1194 alkalinity in Enhanced Weathering experiments. *Applied Geochemistry* 198, 106685.
1195 <https://doi.org/10.1016/j.apgeochem.2026.106685>

1196 Rijnders, J., Vicca, S., Struyf, E., Amann, T., Hartmann, J., Meire, P., Janssens, I., Schoelynck, J.,
1197 2023. The effects of dunite fertilization on growth and elemental composition of barley
1198 and wheat differ with dunite grain size and rainfall regimes. *Front. Environ. Sci.* 11,
1199 1172621. <https://doi.org/10.3389/fenvs.2023.1172621>

1200 Rijnders, J., Vienne, A., Vicca, S., 2025. Effects of basalt, concrete fines, and steel slag on maize
1201 growth and toxic trace element accumulation in an enhanced weathering experiment.
1202 *Biogeosciences* 22, 2803–2829. <https://doi.org/10.5194/bg-22-2803-2025>

1203 Rinder, T., von Hagke, C., 2021. The influence of particle size on the potential of enhanced
1204 basalt weathering for carbon dioxide removal - Insights from a regional assessment.
1205 *Journal of Cleaner Production* 315, 128178.
1206 <https://doi.org/10.1016/j.jclepro.2021.128178>

1207 Rowley, M.C., Grand, S., Verrecchia, É.P., 2018. Calcium-mediated stabilisation of soil organic
1208 carbon. *Biogeochemistry* 137, 27–49. <https://doi.org/10.1007/s10533-017-0410-1>

1209 Rueda, O., Mogollón, J.M., Tukker, A., Scherer, L., 2021. Negative-emissions technology
1210 portfolios to meet the 1.5 °C target. *Global Environmental Change* 67, 102238.
1211 <https://doi.org/10.1016/j.gloenvcha.2021.102238>

1212 Ruiz-Agudo, E., Putnis, C.V., Rodriguez-Navarro, C., Putnis, A., 2012. Mechanism of leached
1213 layer formation during chemical weathering of silicate minerals. *Geology* 40, 947–950.
1214 <https://doi.org/10.1130/G33339.1>

1215 Saleh, H., Braida, W., Zhang, Z., Datta, R., Sarkar, D., 2026. Geochemical fate of lead in
1216 contaminated residential soils following application of amendments for lead
1217 immobilization. *Front Chem* 14, 1742013.
1218 <https://doi.org/10.3389/fchem.2026.1742013>

1219 Sanei, H., Petersen, H.I., Chiaramonti, D., Masek, O., 2025. Evaluating the two-pool decay
1220 model for biochar carbon permanence. *Biochar* 7, 9. [https://doi.org/10.1007/s42773-](https://doi.org/10.1007/s42773-024-00408-0)
1221 [024-00408-0](https://doi.org/10.1007/s42773-024-00408-0)

1222 Schmidt, H.-P., Abiven, S., Cowie, A., Glaser, B., Joseph, S., Kammann, C., Lehmann, J., Leifeld,
1223 J., Pan, G., Rasse, D., Rumpel, C., Woolf, D., Zimmerman, A.R., Hagemann, N., 2025.
1224 Biochar Permanence—A Policy Commentary. *GCB Bioenergy* 17, e70092.
1225 <https://doi.org/10.1111/gcbb.70092>

1226 Schmidt, H.-P., Abiven, S., Hagemann, N., 2022. Permanence of soil applied biochar. An
1227 executive summary for Global Biochar Carbon Sink certification. *The Biochar Journal*
1228 69–74.

1229 Schmidt, H.-P., Anca-Couce, A., Hagemann, N., Werner, C., Gerten, D., Lucht, W., Kammann,
1230 C., 2019. Pyrogenic carbon capture and storage. *GCB Bioenergy* 11, 573–591.
1231 <https://doi.org/10.1111/gcbb.12553>

1232 Schmidt, H.-P., Kammann, C., Hagemann, N., 2024. Certification of the carbon sink potential
1233 of biochar.

1234 Schmidt, H.-P., Kammann, C., Hagemann, N., Leifeld, J., Bucheli, T.D., Sánchez Monedero,
1235 M.A., Cayuela, M.L., 2021. Biochar in agriculture – A systematic review of 26 global
1236 meta-analyses. *GCB Bioenergy* 13, 1708–1730. <https://doi.org/10.1111/gcbb.12889>

1237 Setia, R., Rengasamy, P., Marschner, P., 2014. Effect of mono- and divalent cations on sorption
1238 of water-extractable organic carbon and microbial activity. *Biol Fertil Soils* 50, 727–
1239 734. <https://doi.org/10.1007/s00374-013-0888-1>

1240 Shukla, P.R., Skea, J., Calvo Buendia, E., Masson-Delmotte, V., Pörtner, H.-O., Roberts, D.C.,
1241 Zhai, P., Slade, R., Connors, S.L., van Diemen, R., Ferrat, M., Haughey, E., Luz, S., Neogi,
1242 S., Pathak, M., Petzold, J., Portugal-Pereira, J., Vyas, P., Huntley, E., Kissick, K.,
1243 Belkacemi, M., Malley, J. (Eds.), 2022. *Climate Change and Land: IPCC Special Report*
1244 *on Climate Change, Desertification, Land Degradation, Sustainable Land Management,*
1245 *Food Security, and Greenhouse Gas Fluxes in Terrestrial Ecosystems*, 1st ed. Cambridge
1246 University Press. <https://doi.org/10.1017/9781009157988>

1247 Sinsabaugh, R.L., Manzoni, S., Moorhead, D.L., Richter, A., 2013. Carbon use efficiency of
1248 microbial communities: stoichiometry, methodology and modelling. *Ecology Letters*
1249 16, 930–939. <https://doi.org/10.1111/ele.12113>

1250 Smith, S.M., Fuss, S., Buck, H., Schenuit, F., Pongratz, J., Schulte, I., Lamb, W.F., Probst, B.,
1251 Edwards, M., Nemet, G.F., Cox, E., Vaughan, N., Injy Johnstone, Geden, O., Burke, J.,
1252 Gidden, M., Roe, S., Müller-Hansen, F., Minx, J., 2024. *The State of Carbon Dioxide*
1253 *Removal - 2nd Edition*. OSF.

1254 Sohng, J., Sokol, N.W., Whiteaker, S., Schmidt, R., Holzer, I., Goertzen, H., Peña, J., Houlton,
1255 B.Z., Montañez, I., O’Geen, A., Scow, K., 2025. Combining organic amendments with
1256 enhanced rock weathering shifts soil carbon storage in croplands. *Science of The Total*
1257 *Environment* 998, 180179. <https://doi.org/10.1016/j.scitotenv.2025.180179>

1258 Steinwider, L., Boito, L., De Schutter, A., Frings, P.J., Miladinović, N., Niron, H., Rijnders, J.,
1259 Roussard, J., Van Acker, K., Van Gerven, T., Vienne, A., Watjanatepin, P., Vicca, S., 2026.
1260 Higher Inorganic CO₂ Removal Despite Slower Weathering in an Enhanced Weathering
1261 Experiment With Steel Slags and Basalt. *Global Change Biology* 32, e70666.
1262 <https://doi.org/10.1111/gcb.70666>

1263 Steinwider, L., Boito, L., Frings, P.J., Niron, H., Rijnders, J., de Schutter, A., Vienne, A., Vicca,
1264 S., 2025. Beyond Inorganic C: Soil Organic C as a Key Pathway for Carbon Sequestration
1265 in Enhanced Weathering. *Global Change Biology* 31, e70340.
1266 <https://doi.org/10.1111/gcb.70340>

1267 Su, C., Kang, R., Huang, W., Wang, A., Li, X., Huang, K., Zhou, Q., Fang, Y., 2025. CO₂ removal
1268 with enhanced wollastonite weathering in acidic and calcareous soils. *Soil Ecol. Lett.* 7,
1269 240273. <https://doi.org/10.1007/s42832-024-0273-z>

1270 Sun, F., Lu, S., 2014. Biochars improve aggregate stability, water retention, and pore-space
1271 properties of clayey soil. *Journal of Plant Nutrition and Soil Science* 177, 26–33.
1272 <https://doi.org/10.1002/jpln.201200639>

1273 Swoboda, P., Döring, T.F., Hamer, M., 2022. Remineralizing soils? The agricultural usage of
1274 silicate rock powders: A review. *Science of The Total Environment* 807, 150976.
1275 <https://doi.org/10.1016/j.scitotenv.2021.150976>

1276 Tan, K.H., 2010. *Principles of Soil Chemistry*, 0 ed. CRC Press.
1277 <https://doi.org/10.1201/9781439894606>

1278 Te Pas, E.E.E.M., Chang, E., Marklein, A.R., Comans, R.N.J., Hagens, M., 2025. Accounting for
1279 retarded weathering products in comparing methods for quantifying carbon dioxide
1280 removal in a short-term enhanced weathering study. *Front. Clim.* 6, 1524998.
1281 <https://doi.org/10.3389/fclim.2024.1524998>

1282 Te Pas, E.E.E.M., Comans, R.N.J., Bisseling, S., Hagens, M., 2026. Enhanced weathering and
1283 biochar co-deployment boosts CO₂ sequestration through changing soil properties.
1284 *Geoderma* 466, 117668. <https://doi.org/10.1016/j.geoderma.2025.117668>

1285 Te Pas, E.E.E.M., Hagens, M., Comans, R.N.J., 2023. Assessment of the enhanced weathering
1286 potential of different silicate minerals to improve soil quality and sequester CO₂. *Front.*
1287 *Clim.* 4, 954064. <https://doi.org/10.3389/fclim.2022.954064>

1288 Vicca, S., Goll, D.S., Hagens, M., Hartmann, J., Janssens, I.A., Neubeck, A., Peñuelas, J.,
1289 Poblador, S., Rijnders, J., Sardans, J., Struyf, E., Swoboda, P., Van Groenigen, J.W.,
1290 Vienne, A., Verbruggen, E., 2022. Is the climate change mitigation effect of enhanced
1291 silicate weathering governed by biological processes? *Global Change Biology* 28, 711–
1292 726. <https://doi.org/10.1111/gcb.15993>

1293 Vienne, A., Frings, P., Poblador, S., Steinwider, L., Rijnders, J., Schoelynck, J., Vinduskova, O.,
1294 Vicca, S., 2024. Earthworms in an enhanced weathering mesocosm experiment: Effects
1295 on soil carbon sequestration, base cation exchange and soil CO₂ efflux. *Soil Biology*
1296 *and Biochemistry* 199, 109596. <https://doi.org/10.1016/j.soilbio.2024.109596>

1297 Vienne, A., Frings, P., Rijnders, J., Boito, L., Hartmann, J., Niron, H., Poetra, R., Estrada, M.P.,
1298 Reershemius, T., Steinwider, L., Suhrhoff, T.J., Vicca, S., 2026a. Weathering without
1299 realizing inorganic CO₂ removal revealed through base cation monitoring. *SOIL* 12,
1300 421–440. <https://doi.org/10.5194/soil-12-421-2026>

1301 Vienne, A., Newell, J., Roussard, J., Doherty, R., Cox, S.F., Lyons, G., Vicca, S., 2026b. Effects of
1302 basalt and biochar addition on base cations and trace metals in plants and soil in an
1303 urban field trial. *Biogeosciences* 23, 1681–1695. <https://doi.org/10.5194/bg-23-1681-2026>

1304

1305 Vienne, A., Poblador, S., Portillo-Estrada, M., Hartmann, J., Ijehon, S., Wade, P., Vicca, S.,
1306 2022. Enhanced Weathering Using Basalt Rock Powder: Carbon Sequestration, Co-
1307 benefits and Risks in a Mesocosm Study With *Solanum tuberosum*. *Front. Clim.* 4,
1308 869456. <https://doi.org/10.3389/fclim.2022.869456>

1309 Vorrath, M.-E., Amann, T., Meyer zu Drewer, J., Hagemann, N., Aldrich, C., Börker, J., Seedtke,
1310 M., Becker, J.N., Hagens, M., Eschenbach, M., Hartmann, J., 2025. Pyrogenic carbon
1311 and Carbonating Minerals for Carbon Capture and Storage (PyMiCCS) Part II: Organic
1312 and Inorganic Carbon Dioxide Removal in an Oxisol. *Frontiers in Climate.*
1313 <https://doi.org/10.3389/fclim.2025.1592454>

1314 Vorrath, M.-E., Amann, T., Meyer zu Drewer, J., Linke, T., Feiertag, L., Nauenburg, S.,
1315 Maslouski, M., Ansari, M., Eschenbach, A., Hagemann, N., Hartmann, J., in prep.
1316 Soil-Dependent Controls of Carbon Dioxide Removal from combined Enhanced Rock
1317 Weathering and Biochar in different Soils. *Applied Geochemistry*.

1318 Vorrath, M.-E., Haque, F., Stoeck, L., Aldrich, C., Kiddell, M., Smet, I., in prep. Hot, hotter,
1319 thermal activation: how to boost weathering rates of serpentine-rich rocks for carbon
1320 dioxide removal. *Data in Brief*.

1321 Wang, J., Xiong, Z., Kuzyakov, Y., 2016. Biochar stability in soil: meta-analysis of decomposition
1322 and priming effects. *GCB Bioenergy* 8, 512–523. <https://doi.org/10.1111/gcbb.12266>

1323 Wang, Y., Wang, H.-S., Tang, C.-S., Gu, K., Shi, B., 2022. Remediation of heavy-metal-
1324 contaminated soils by biochar: a review. *Environmental Geotechnics* 9, 135–148.
1325 <https://doi.org/10.1680/jenge.18.00091>

1326 Wang, Y., Xiao, X., Chen, B., 2018. Biochar Impacts on Soil Silicon Dissolution Kinetics and their
1327 Interaction Mechanisms. *Sci Rep* 8, 8040. [https://doi.org/10.1038/s41598-018-26396-](https://doi.org/10.1038/s41598-018-26396-3)
1328 [3](https://doi.org/10.1038/s41598-018-26396-3)

1329 Wang, Z.-L., Li, Y.-F., Jiang, P.-K., Zhou, G.-M., Liu, J., 2014. Effect of bamboo leaf biochar
1330 addition on soil CO₂ efflux and labile organic carbon pool in a Chinese chestnut
1331 plantation. *Ying Yong Sheng Tai Xue Bao* 25, 3152–3160.

1332 Waring, B.G., Gurgel, A., Köberle, A.C., Paltsev, S., Rogelj, J., 2023. Natural Climate Solutions
1333 must embrace multiple perspectives to ensure synergy with sustainable development.
1334 *Front. Clim.* 5, 1216175. <https://doi.org/10.3389/fclim.2023.1216175>

1335 West, T.O., McBride, A.C., 2005. The contribution of agricultural lime to carbon dioxide
1336 emissions in the United States: dissolution, transport, and net emissions. *Agriculture,*
1337 *Ecosystems & Environment* 108, 145–154.
1338 <https://doi.org/10.1016/j.agee.2005.01.002>

1339 Wilson, M.J., 1999. The origin and formation of clay minerals in soils: past, present and future
1340 perspectives. *Clay Minerals* 34, 7–25. <https://doi.org/10.1180/000985599545957>

1341 Xu, T., Yuan, Z., Vicca, S., Goll, D.S., Li, G., Lin, L., Chen, H., Bi, B., Chen, Q., Li, C., Wang, X.,
1342 Wang, C., Hao, Z., Fang, Y., Beerling, D.J., 2024. Enhanced silicate weathering
1343 accelerates forest carbon sequestration by stimulating the soil mineral carbon pump.
1344 *Global Change Biology* 30, e17464. <https://doi.org/10.1111/gcb.17464>

1345 Yang, F., Xu, Z., Huang, Y., Tsang, D.C.W., Ok, Y.S., Zhao, L., Qiu, H., Xu, X., Cao, X., 2021.
1346 Stabilization of dissolvable biochar by soil minerals: Release reduction and organo-
1347 mineral complexes formation. *Journal of Hazardous Materials* 412, 125213.
1348 <https://doi.org/10.1016/j.jhazmat.2021.125213>

1349 Yu, Y., Liu, D., Wu, H., 2014. Formation and Characteristics of Reaction Intermediates from the
1350 Fast Pyrolysis of NaCl- and MgCl₂-Loaded Celluloses. *Energy Fuels* 28, 245–253.
1351 <https://doi.org/10.1021/ef401483u>

1352 Zhu, C., Huang, K., Xue, M., Zhang, Y., Wang, J., Liu, L., 2023. Effect of MgCl₂ Loading on the
1353 Yield and Performance of Cabbage-Based Biochar. *Bioengineering (Basel)* 10, 836.
1354 <https://doi.org/10.3390/bioengineering10070836>
1355

1 **Supplementary Information**

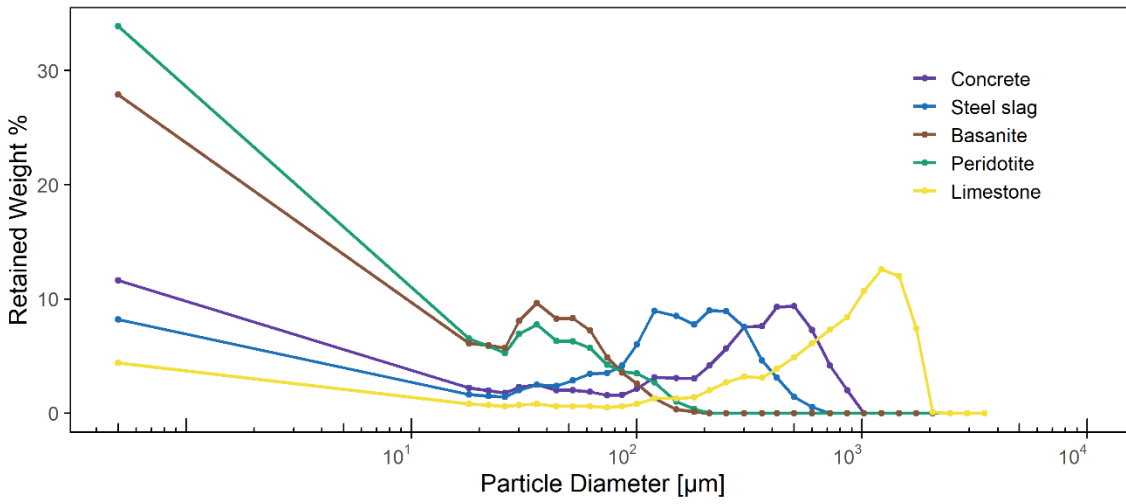
2 **Table of content**

3	S1. Grain size distribution	2
4	S2. Pyrolysis of biochar and RE-biochars and hydrolysis	3
5	S3. Characteristics of the sand soil	4
6	S4. Experimental setup	5
7	S5. Leachate analyses	7
8	S6. Calculations of chemical fluxes, alkalinity production rates, different carbon sinks and the	
9	soil carbon and cation budgets.....	9
10	S7. Trace metal fluxes.....	16
11	S8. Cation budget in the soil.....	18
12	S9. Correlation of magnesium and carbon conversion from wet-impregnation	19
13	S10. Description of qualitative assessment of soil amendments.....	20
14	S11. Timeseries of net DOC fluxes, bulk chemistry, cations and anions.....	22
15	S12. Time series of leachate analyses	23
16	References	26

17

18

19 S1. Grain size distribution



20

21 Figure S1. Grain size distribution of mineral feedstock samples concrete, steel slag, basanite, peridotite
22 and limestone.

23

24 S2. Pyrolysis of biochar and RE-biochars and hydropyrolysis

25 *Pyrolysis*

26 All biochar and RE-biochars were pyrolyzed in a PYREKA pyrolysis unit from *Novocarbo* in Dörth,
27 Germany. The PYREKA unit consists of a continuous auger reactor with a diameter of 8cm. The
28 reactor is purged with N₂ at flowrates of 2.5 L min⁻¹. To achieve the highest heating temperature
29 of the pyrolysis process, the reactor is heated to 650°C. All thermal conversions were carried out
30 at this temperature, with a residence time of approx. 15 minutes. To ensure that there is no
31 intrusion of oxygen or disruptions in the reactor temperature, the feedstock inlet is separated
32 from the reactor by a rotary valve. After the pyrolysis process, the resulting materials are cooled
33 down to ambient temperatures while being protected from oxygen exposure. This is achieved by
34 utilizing the N₂ purged outlet of the PYREKA unit.

35 *Hydropyrolysis*

36 Hydropyrolysis (HyPy) was conducted as outlined by Meredith et al. (2017). In summary, milled
37 samples were combined with 10 wt% ammonium molybdate-tetrahydrate as a catalyst. The
38 samples were heated in a reactor under 150 bar of hydrogen pressure, starting from ambient
39 temperature to 250 °C at a rate of 300 °C min⁻¹. They were then raised from 250 °C to 550 °C at
40 8 °C min⁻¹ and maintained at that temperature for 2 minutes. The residues after HyPy were
41 weighed and analysed for C_{org}. This residue is categorized as stable polycyclic aromatic carbon,
42 containing more than 7 fused aromatic rings that exhibit high environmental stability (Schmidt
43 et al., 2022). This mass remaining of the initial C_{org} content is expressed as BC_{HyPy}.

44

45

46 **S3. Characteristics of the sand soil**

47 Table S1. Key properties and grain-size distribution of the sandy soil. All data and methodological details
48 are reported in Ansari et al. (2026).

Physico-chemical properties				Grain size distribution in wt%	
pH in H ₂ O			5.6	Coarse sand	2.3
pH in CaCl ₂			4.7	Middle sand	50
Electric conductivity	$\mu\text{S cm}^{-1}$		47.7	Coarse fine sand	33.3
Total carbon	wt%		1.24	Fine fine sand	8.1
Total inorganic carbon	wt%		0.04	Coarse silt	1.2
Organic carbon	wt%		1.2	Middle silt	0.8
Total nitrogen	wt%		0.1	Fine silt	0.5
OC/N _{tot}			11.3	Clay	3.7
Cation exchange capacity	mmolc kg ⁻¹		21		
Base saturation	%		140.7		
Water capacity	%		0.6		
Water holding capacity	%		35.5		

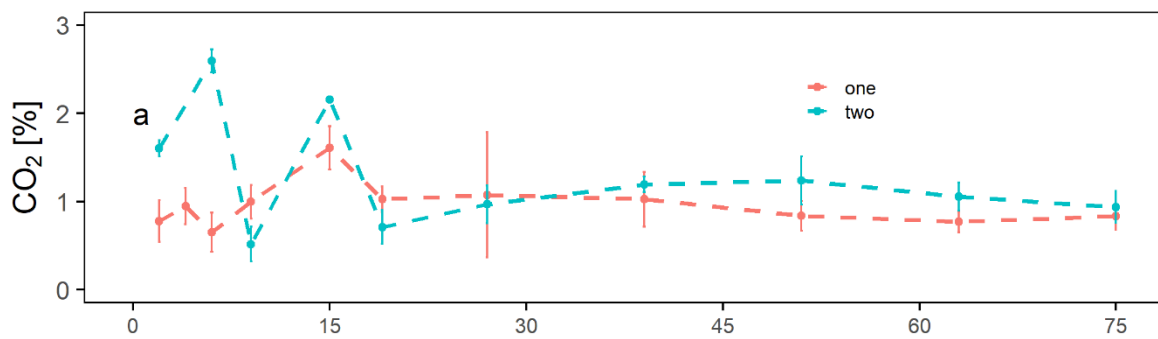
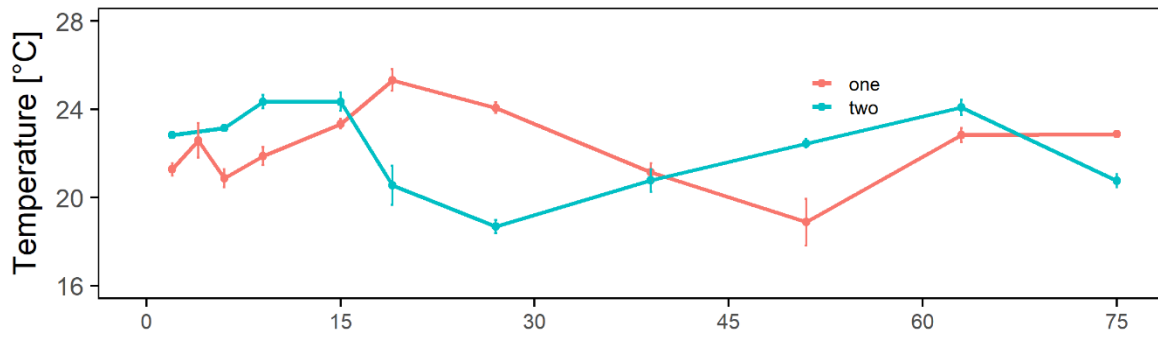
49

50

51 S4. Experimental setup

52 To initiate the incubation process, acrylic tubes were used as soil columns (25 mm length, 56 mm
53 inner diameter) that were sealed at the bottom with a 5 μm plankton net. For each batch,
54 duplicates of 500 g of sand were mixed with a specific material, filled into the columns, and lightly
55 tapped to allow the soil to settle. For single and co-applications either 10g of biochar and/or 9.9g
56 of mineral were used, for RE-biochars the mass of material was adjusted to contain 9.9g of
57 mineral which resulted in 15 to 16.3g. The single materials, the co-deployment of biochar and
58 minerals as well as RE-biochars and several control columns made up 38 columns in total. The
59 columns were placed vertically in two gas-sealed incubators which were regularly flushed with a
60 N_2+CO_2 gas mixture to maintain an atmosphere of pCO_2 of 1.5%. Due to diffusion of gas a CO_2
61 level of $1.0\% \pm 0.4$ (box 1) and $1.2\% \pm 0.6$ (box 2) was maintained over the experiment period
62 (Figure S2). Prior to the experiment, the columns were saturated by soaking them with 250 ml of
63 deionised water (DI). During the experiment, the columns were rinsed with DI, which had been
64 gasified with the corresponding N_2+CO_2 gas mixture until equilibration. This process aimed to
65 simulate rainwater in equilibrium with the pCO_2 of the soil environment within the incubator.
66 According to PhreeqC, the target values were a pH of 4.806 and an EC of $5 \mu\text{S cm}^{-1}$ at 20°C . To
67 mimic an annual rainfall of 820 mm, the columns were rinsed three times a week with 12.9 ml of
68 DI. The leachate water resulting from this rinsing process was collected in 250 ml polyethylene
69 bottles positioned beneath the columns. The experiments were carried out over a period of 75
70 weeks in a dark room, maintaining an approximate temperature of $22.3^\circ\text{C} \pm 1.8$. Sampling
71 intervals were progressively extended over time, starting at two-week intervals and increasing to
72 twelve-week intervals. The specific sampling weeks were as follows: week 2, 4, 6, 9, 15, 19, 27,
73 39, 51, 63 and 75. The first box was also sampled in week 87 but this data was only for chemical
74 flux monitoring (Figure S7-9 in S11-12) and not used for any calculations in this study.

75



76

77 Figure S2. Temperature and CO₂ levels in the incubator boxes during the experiment. Error bars indicate
 78 standard deviations, n=18.

79

80 S5. Leachate analyses

81 The sampling and analyses of the leachates during the incubation experiment were done
82 according to Vorrath et al. (2025). At each sampling time, dissolved inorganic carbon (DIC) was
83 sampled directly inside the incubator to prevent re-equilibration with the lab atmosphere. Trace
84 metals were as well sampled directly inside the incubator, acidified (1 ml of 14 M HNO₃) and
85 pooled after experiment weeks 9 and 27. Outside the incubator, pH, temperature, and EC of the
86 leachate were immediately measured with a WTW 3630 IDS Multimeter. For total alkalinity (TA),
87 major ion chromatography, and dissolved silica (DSi), samples were passed through a 0.45 µm
88 PES syringe filter and analysed within 48 hours to reduce changes caused by precipitation of
89 minerals that may be supersaturated. Samples for dissolved organic carbon (DOC) were filtered
90 using pre-combusted glass fibre filters with an approximate pore size of 0.45 µm (Whatman
91 GF/F). All samples were kept cool and protected from light until analysis. Additionally, pH, EC, TA,
92 and major ions were also determined for the mineral suspension in the same way.

93 The analyses of DIC, TA, DSi, DOC and major ions was described in Vorrath et al. (2025). DIC
94 samples were analysed using a Picarro G2131-I cavity ring-down spectrometer coupled with an
95 AutoMate FX preparation device. Total alkalinity was determined via automated titration to pH
96 4.3 using a Metrohm Titrando titrator with 0.02 N HCl, following the procedure described by
97 Dickson (1981). Calibration was performed against two in-house standards, with an error margin
98 below 1%. Major cations (Na⁺, K⁺, Ca²⁺, Mg²⁺) and anions (Cl⁻, SO₄²⁻) were analysed through ion
99 chromatography using a Metrohm 881 Compact IC Pro system, achieving an error rate of less
100 than 5%. Dissolved silica was measured using the molybdate blue colorimetric method as
101 described by Hansen and Koroleff (1999). The average coefficient of variation for all
102 measurements was 0.6 ± 0.8%. DOC concentrations were determined with a Shimadzu TOC-VCSH
103 Analyzer, utilizing high-temperature combustion and non-dispersive infrared detection. The
104 trace metals copper (Cu), chromium (Cr), cadmium (Cd), lead (Pb), and nickel (Ni) were
105 determined via atomic absorption spectroscopy (AAS). The instrument was calibrated using
106 appropriate standard solutions by measuring absorbance at specific wavelengths (Cu at 324.7
107 nm, Cr at 357.9 nm, Cd at 228.8 nm, Pb at 283.3 nm, and Ni at 232.0 nm) and metal concentration

108 of each sample was quantified by comparison to these standards. Acceptable errors were within
109 0.5%.

110 S6. Calculations of chemical fluxes, alkalinity production rates, different carbon sinks
111 and the soil carbon and cation budgets

112 *Chemical fluxes*

113 The fluxes of element x (F_x) per interval I is calculated following Amann et al. (2022)

$$F_{x,i} = (c_{x,i} * Q_{rain,i}) / t_i \quad \text{Eq. 1}$$

114 Where c_x represents the element concentration (mol L⁻¹), Q_{rain} (L) is the volume of irrigation per
115 interval, and t_i is the number of weeks per interval (days). To calculate the total elements released
116 over the experiment duration of 75 weeks they are summed as:

$$F_{tot,i} = \sum_{t=1}^{75} F_{x,i} \quad \text{Eq. 2}$$

117

118 *Alkalinity production rates*

119 For all inorganic carbon fluxes, the carbonate alkalinity (CA) was derived from measured values
120 of DIC, pH, temperature, and cation concentrations using Phreeqc (Parkhurst and Appelo, 2013)
121 (database: phreeqc.dat) to exclude contributions from organic alkalinity (Rieder et al., 2026). The
122 weekly net production rate of carbonate alkalinity (CA_{prod}) per unit mass of soil amendment was
123 calculated using the amount of CA released, according to the following equation:

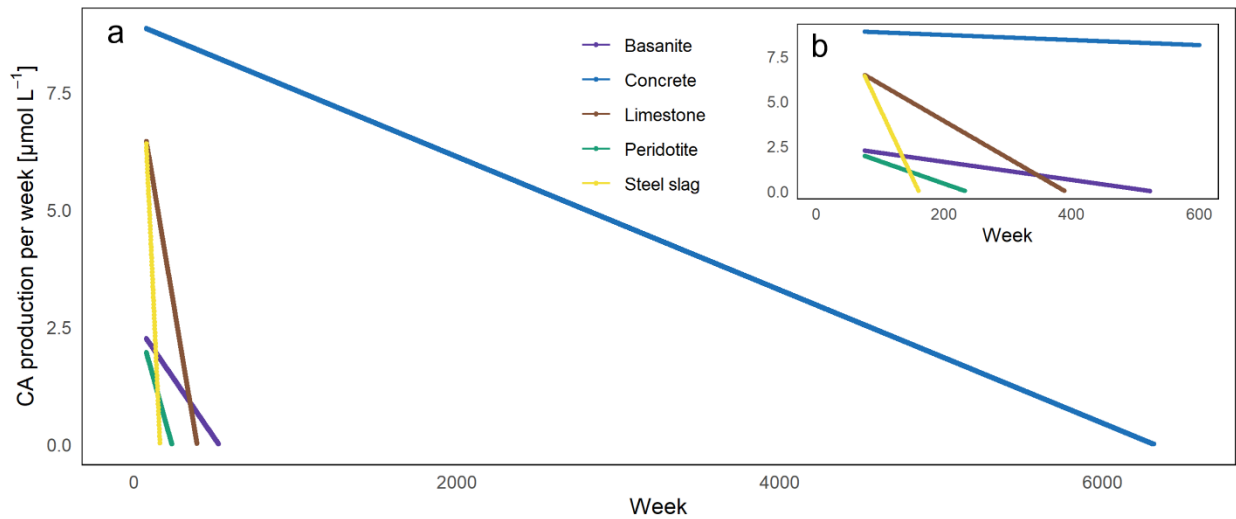
$$CA_{prod} = Q_{rain}(t_i) \times c_{TA}(t_i) * \frac{mass_{amendment}}{100} \div t_i \quad \text{Eq. 3}$$

124 where Q_{rain} (L) represents the irrigation volume per column during sampling interval t_i, c_{CA} (mol
125 L⁻¹) is the CA at time t_i, mass_{amendment} (g) refers to the mass of the respective soil amendment, and
126 t_i denotes the number of weeks since the previous sampling event. The net CA_{prod} was used to
127 extrapolate mineral weathering of rock amendments and determine after how many weeks the
128 values reached 0 and how much CA had been released in this time. For this, only CA_{prod} values of
129 weeks 39-75 were used to generate a linear model for each amendment (a + b*week, Table S2)
130 as in this time a stable alkalinity flux was observed. This model was then used to estimate the
131 duration during which CA_{prod} indicated positive net fluxes.

132 Table S2: Coefficients a and b derived from the linear model for each mineral amendment to be used for
 133 a linear extrapolation of $CA_{prod} = a * week + b$.

	a	b
Concrete	-0.001	8.966
Steel slag	-0.076	12.169
Basanite	-0.005	2.630
Peridotite	-0.012	2.897
Limestone	-0.021	8.015

134



135

136 Figure S3: Extrapolation of the carbonate alkalinity production (CA_{prod}) of mineral feedstocks. a) The
 137 extrapolation starts in week 76 and runs until CA_{prod} reaches 0 for each individual material. The
 138 extrapolation of concrete had to be stopped in week 2022 when the full IC-Sink_{pot} was realised. b) Detailed
 139 view on the first 600 weeks of extrapolation.

140

141 *Calculations of potential carbon sinks*

142 The potential carbon sink from inorganic carbon based on alkalinity release from mineral
 143 weathering, the IC-Sink (IC-Sink_{pot}, kgCO₂ t⁻¹), was calculated by:

$$IC - Sink_{pot} \text{ of Rock} = \frac{Rock_{fraction}}{100} * CDR_{rock \text{ powder}} \quad \text{Eq. 4}$$

144 where the rock fraction of the amended material is $Rock_{fraction}$ (%), and $CDR_{rock\ powder}$ ($kgCO_2\ t^{-1}$) is
 145 the CDR potential of the according rock powder calculated after Renforth (2019) (values see
 146 supplementary data D2). Neither for the CDR potential nor for the IC-sinks was the potential
 147 downstream CO_2 loss due to surface water re-equilibration as proposed by Renforth (2019)
 148 applied to keep CO_2 values comparable to values from DOC in this study and comparable to other
 149 studies in general. Since the experiments were performed in darkness without plants or fauna,
 150 nutrient uptake was not considered (Dietzen and Rosing, 2023).

151 The IC-Sink_{pot} from inorganic carbon based on alkalinity release from biochar is calculated as

$$IC - Sink_{pot\ of\ Biochar} = \frac{Biochar_{fraction} * PIC_{biochar}}{100} / M_C * M_{CO_2} \quad Eq. 5$$

152 where the fraction of biochar is $Biochar_{fraction}$ (%) and the particulate inorganic carbon (PIC) in
 153 biochar is $PIC_{biochar}$ (%). The molar masses are defined as $44.01\ g\ mol^{-1}$ for CO_2 (M_{CO_2}) and $12.01\ g$
 154 mol^{-1} , for carbon (M_C).

155 The IC-Sink_{pot} from inorganic carbon based on alkalinity release from biochar carbonates in RE-
 156 biochars is calculated as

$$\begin{aligned}
 & IC - Sink_{pot\ of\ RE - Biochar} \\
 &= \frac{Biochar_{fraction}}{100} \\
 & \quad \frac{\left(\frac{Biochar_{fraction} * PIC_{biochar}}{100} \right) - \left(\frac{Rock_{fraction} * PIC_{rock}}{100} \right)}{Biochar_{fraction} * 100} \\
 & \quad * \frac{1}{100} \\
 & \quad / M_C * M_{CO_2}
 \end{aligned} \quad Eq. 5$$

157 by utilizing the fractions of rock in RE-biochars ($Rock_{fraction}$, %) and the particulate inorganic
 158 carbon (PIC) of the rock (PIC_{rock} , %), and with the RE-biochar fraction ($RE-biochar_{fraction}$, %), the
 159 PIC in RE-biochar ($PIC_{RE-biochar}$, %), and the fraction of biochar ($Biochar_{fraction}$, %) in RE-biochar. The
 160 molar mass of CO_2 M_{CO_2} is $44.01\ g\ mol^{-1}$ and of carbon M_C is $12.01\ g\ mol^{-1}$.

161 The carbon sink from pyrogenic carbon in biochar, the PyC-Sink, at the day of application was
 162 calculated with:

$$PyC - Sink = \frac{C_{org(RE-)}biochar}{100} * \frac{100 - (RE -)biochar_{ashfraction}}{100} / M_C * M_{CO_2} \quad Eq. 7$$

163 with the C_{org} of all (RE-)biochars ($C_{org(RE-)}biochar$, %), the ash fraction of (RE-)biochars ((RE-
 164) $biochar_{ashfraction}$, %), and the molar mass of CO_2 M_{CO_2} (44.01 g mol⁻¹) and carbon M_C
 165 (12.01 g mol⁻¹). For an estimation of long-term carbon storage, the $PyC-Sink_{long}$ was multiplied
 166 with the amount of BC_{HyPy} from the HyPy analysis. To avoid overestimation, the C_{org} decay
 167 considered to happen over 1000 years was also applied on the experiment duration of 75 weeks
 168 as most of the $PyC-Sink$ loss occurs within the first year of soil application.

169 For the total $C-Sink_{pot}$, the $IC-Sink_{pot}$ of rock, biochar or RE-biochar and the $PyC-Sink_{pot}$ are
 170 summed according to their fraction in the amendment.

171 To calculate the equivalent of CO_2 from concentration of DOC (c_{DOC}) in the leachate water, the
 172 measured DOC is multiplied with 44.01 g mol⁻¹ for CO_2 (M_{CO_2}).

$$CO_2 \text{ from DOC} = c_{DOC} * M_{CO_2} \quad Eq. 8$$

173

174 *Calculation of deviations of measured from expected C-Sinks*

175 To identify synergistic effects, the deviation of the measured from the expected C-Sinks (carbon
 176 sinks from both inorganic and pyrogenic carbon) of co-application and (RE-)biochar amendments
 177 is estimated based on individual biochar and mineral amendment. The expected C-Sink
 178 ($C-Sink_{expected}$) is determined as:

$$\begin{aligned} C - Sink_{expected} & \quad Eq. 9 \\ & = (IC - sink_{pure \text{ biochar}} * \text{biochar content}) \\ & + (IC - sink_{pure \text{ rock}} * \text{rock content}) \\ & + (PyC - sink * \text{biochar content}) \end{aligned}$$

179 where, for every specific soil amendment, the $IC-Sink$ of the single biochar amendment
 180 ($IC-Sink_{pure \text{ biochar}}$) is multiplied with the biochar content, the $IC-Sink$ of the single rock amendment
 181 ($IC-Sink_{pure \text{ rock}}$) is multiplied with the rock content and the $PyC-Sink$ is multiplied with the biochar

182 content. To calculate the expected IC-Sink ($IC-Sink_{expected}$) the PyC-Sink is not considered in the
183 equation.

184 The deviation of the measured C-Sink from the expected C-Sink is calculated as:

$$Deviation\ measured\ C - Sink\ \% = \frac{C-Sink_{measured} - C-Sink_{expected}}{C-Sink_{expected}} * 100 \quad Eq. 10$$

185 where, for every specific soil amendment, the $C-Sink_{measured}$ is the measured value and the
186 $C-Sink_{expected}$ is determined after equation 9.

187 The deviation of the measured IC-Sink and expected IC-Sink is calculated as:

$$Deviation\ measured\ IC - Sink\ \% = \frac{IC - Sink_{measured} - (IC - Sink_{expected\ rock} - IC - Sink_{expected\ biochar})}{IC - Sink_{expected\ rock} + IC - Sink_{expected\ biochar}} * 100 \quad Eq. 11$$

188 where the $IC-Sink_{measured}$ is the measured CA in the leachate and the $IC-Sink_{expected\ rock}$ and
189 $IC-Sink_{expected\ biochar}$ are the expected IC-Sinks of each rock and biochar.

190 To determine the deviation from the measured geogenic IC-Sink from the expected geogenic IC-
191 Sink, the IC-Sink from biochar is treated as a constant and the remaining IC-Sink is attributed to
192 mineral weathering:

$$Deviation\ measured\ geogenic\ IC - sink\ \% = \frac{IC - Sink_{measured} - IC - Sink_{expected\ biochar} - IC - Sink_{expected\ rock}}{IC - Sink_{expected\ rock}} * 100 \quad Eq. 12$$

193

194 *Calculation of soil carbon budget*

195 To assess changes in organic and inorganic soil carbon pools, the initial carbon pool (initial C_{pool})
196 of each soil column was compared to the post-experiment soil column. This comparison
197 considers:

$$Initial C_{pool} = IC_{soil} + C_{org\ soil} + IC_{rock} + C_{org\ rock} + IC_{(RE-)\ biochar} + C_{org\ (RE-)\ biochar} \quad \text{Eq. 13}$$

198 using the inorganic soil carbon (IC_{soil}), the organic soil carbon ($C_{org\ soil}$), the inorganic carbon from
 199 the rock (IC_{rock}), the organic carbon of rock powder ($C_{org\ rock}$), the inorganic carbon from (RE-
 200)biochars ($IC_{(RE-)\ biochar}$) and the organic carbon of (RE-)biochars ($C_{org(RE-)\ biochar}$).

201 The final C_{pool} after the experiment was determined as

$$Final C_{pool} = IC_{soil} + C_{org\ soil} + IC_{leachate} + C_{org\ leachate} \quad \text{Eq. 14}$$

202 with the inorganic soil carbon (IC_{soil}), the organic soil carbon ($C_{org\ soil}$) the sum of inorganic carbon
 203 from all DIC leachate measurements ($IC_{leachate}$) and the sum of C_{org} from all DOC leachate
 204 measurements ($C_{org\ leachate}$).

205

206 *Calculation of major cation budget*

207 The change of the major cation budget throughout the experiment was determined by
 208 comparison of the initial $Cation_{pool}$ to the final $Cation_{pool}$:

$$Initial Cation_{pool} = Cation_{rock} + Cation_{(RE-)\ biochar} + Cation_{soilCECcontrol} \quad \text{Eq. 15}$$

209 with cations added from rock powder ($Cation_{rock}$), and cations added from biochar ($Cation_{(RE-)\ biochar}$)
 210 and $Cation_{soilCECcontrol}$ representing the cations in the control soil leached during the analysis
 211 of cation exchange capacity after the experiment. The final $Cation_{pool}$ is based on

$$Final Cation_{pool} = Cation_{soilCEC} + Cation_{leachate} \quad \text{Eq. 16}$$

212 where $Cation_{soilCEC}$ represents cations leached from exchangeable sites of individual
 213 amendments, and $Cation_{leachate}$ is the sum of the specific cation concentrations from all leachate
 214 measurements. The difference between the initial and final cation pools is assumed to represent
 215 cations retained in a solid phase, either as part of rock, biochar, in secondary mineral formations,
 216 (hydr-)oxides or associated with organic matter.

217

218 *Calculation of deviations from expected trace metal fluxes*

219 The deviation of the expected trace metal fluxes and measured trace metal fluxes is calculated
220 as:

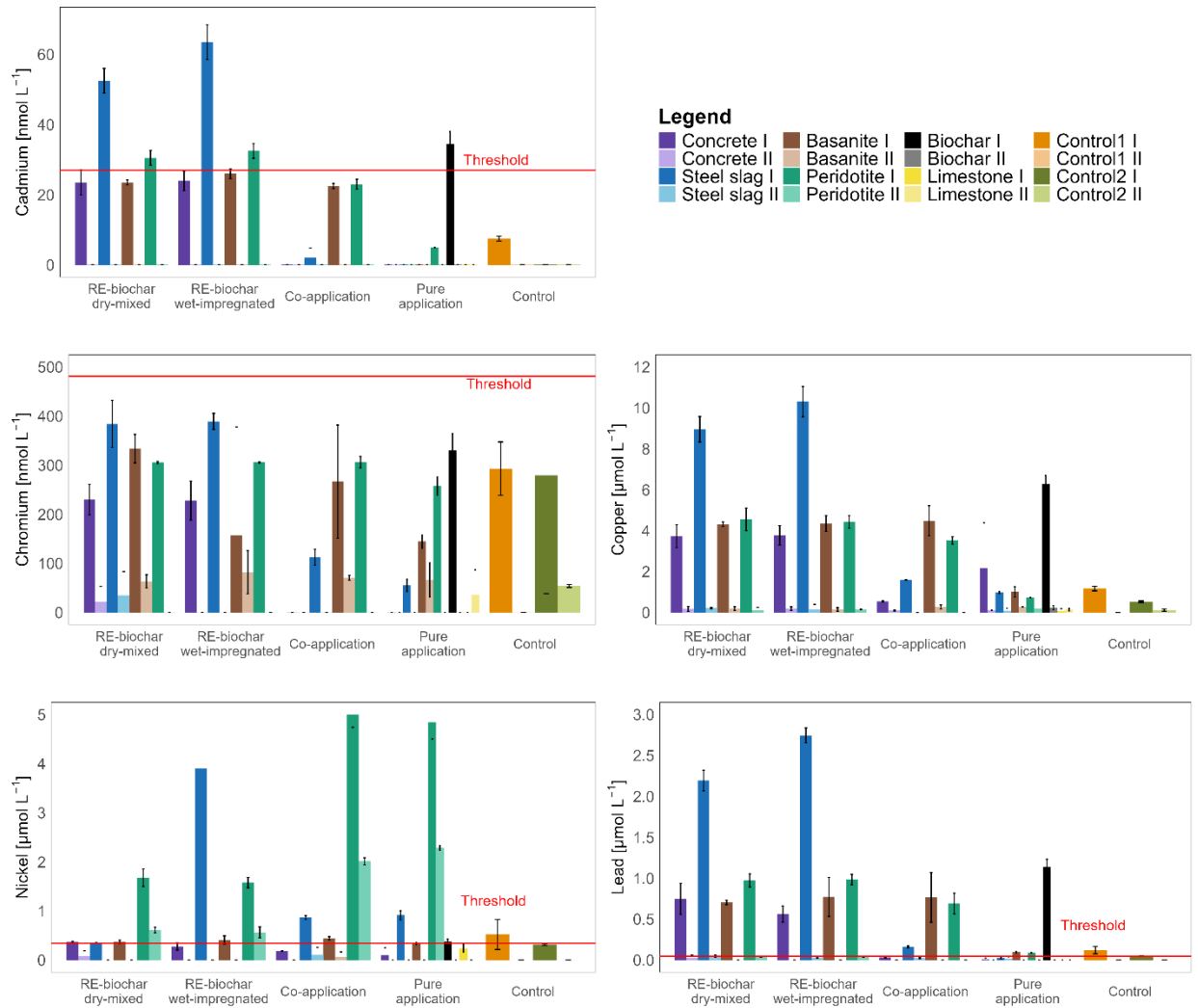
$$\text{Deviation expected TM flux \%} = \frac{(TMflux_{\text{pure rock}} * \text{rockcontent} + TMflux_{\text{pure biochar}} * \text{biocharcontent}) - TMflux_{\text{measured}}}{TMflux_{\text{pure rock}} * \text{rockcontent} + TMflux_{\text{pure biochar}} * \text{biocharcontent}} * 100 \quad \text{Eq. 17}$$

221 where the trace metal fluxes of pure rock ($TMflux_{\text{pure rock}}$) and pure biochar ($TMflux_{\text{pure biochar}}$) are
222 multiplied with their content in the specific amendments, subtracted from the measured trace
223 metal flux ($TMflux_{\text{measured}}$) and divided by the same.

224

225 S7.Trace metal fluxes

226 The concentrations of trace metals show a sharp decline between week 9 and week 27 (indicated
227 with I and II in Figure S4, data in supplementary data D8). Cadmium concentrations were highest
228 for RE-biochar containing steel slag and peridotite as well as single biochar (max. 63.5 nmol L⁻¹).
229 Chromium release was highest in all RE-biochar and co-deployments of basanite and peridotite
230 (maximum 389 nmol L⁻¹), and also both in pure and co-deployment of basanite, peridotite and
231 biochar. Elevated copper and lead concentrations were observed in RE-biochar with steel slag
232 and single biochar reaching up to 3.6 μmol L⁻¹ for copper and 2.7 μmol L⁻¹ for lead. Nickel release
233 was primarily associated with amendments containing peridotite (maximum 5.0 μmol L⁻¹) and
234 steel slag. When compared with the limits of the German Drinking Water Ordinance, trace metal
235 release from several RE-biochars with steel slag and peridotite exceeds the thresholds for
236 cadmium, nickel, and lead (red line in Figure S4). Further, single biochar amendments, concrete
237 RE-biochar and basanite RE-biochar and co-deployments exceed thresholds for several metals.
238 Notably, nickel and lead thresholds were also exceeded in the control soil during the first
239 sampling interval.

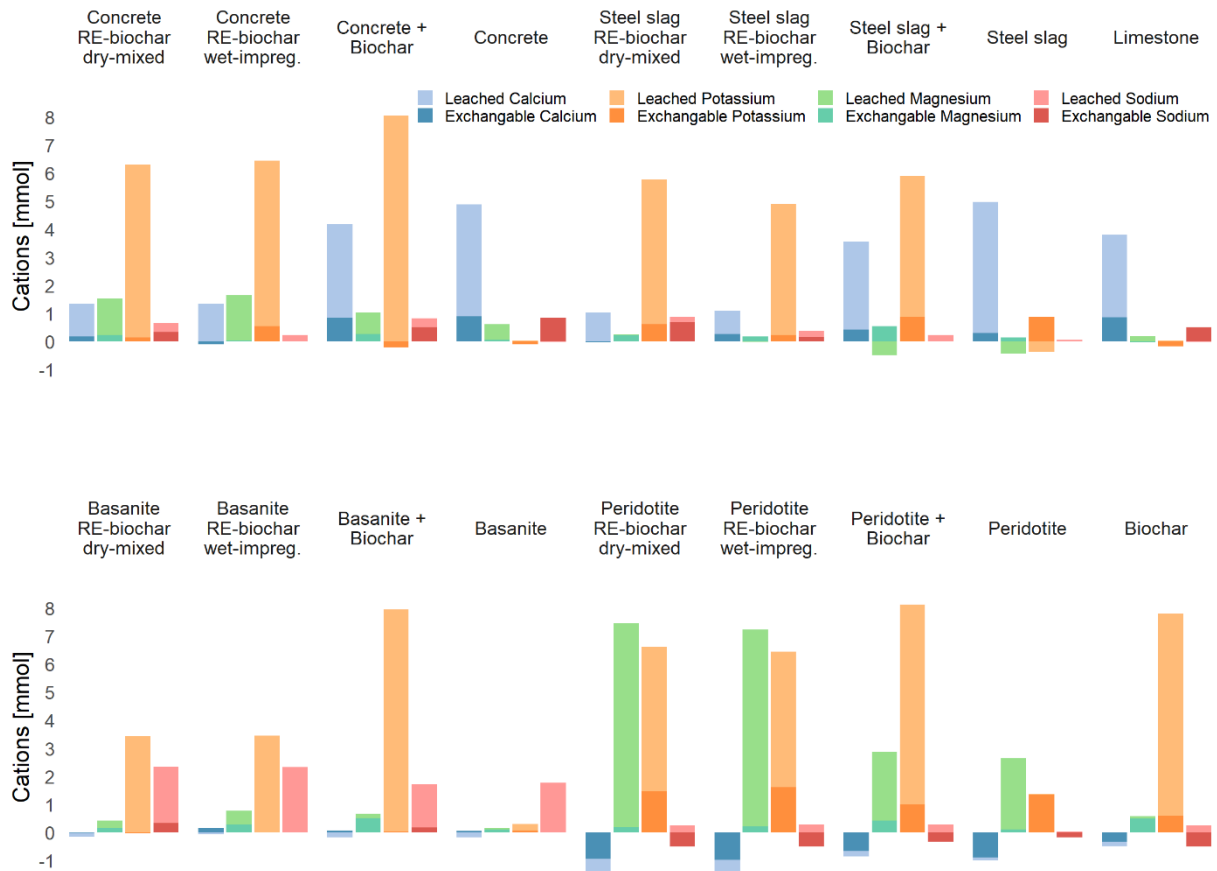


240

241 Figure S4: Concentrations of trace metals from pooled samples after 9 and 27 weeks indicated with I and
 242 II, respectively. The thresholds from the German Drinking Water Ordinance are indicated by the red line
 243 and are 27 nmol L⁻¹ for cadmium, 481 nmol L⁻¹ for chromium, 31.3 μmol L⁻¹ for copper (not shown in the
 244 plot), 0.341 μmol L⁻¹ for nickel, and 0.048 μmol L⁻¹ for lead. Error bars indicate standard deviations (n=2).
 245 Experiments with materials including steel slag, peridotite and biochar were done in box 1 (control 1),
 246 while materials including concrete, basanite and limestone were done in box 2 (control 2).

247

248 S8. Cation budget in the soil

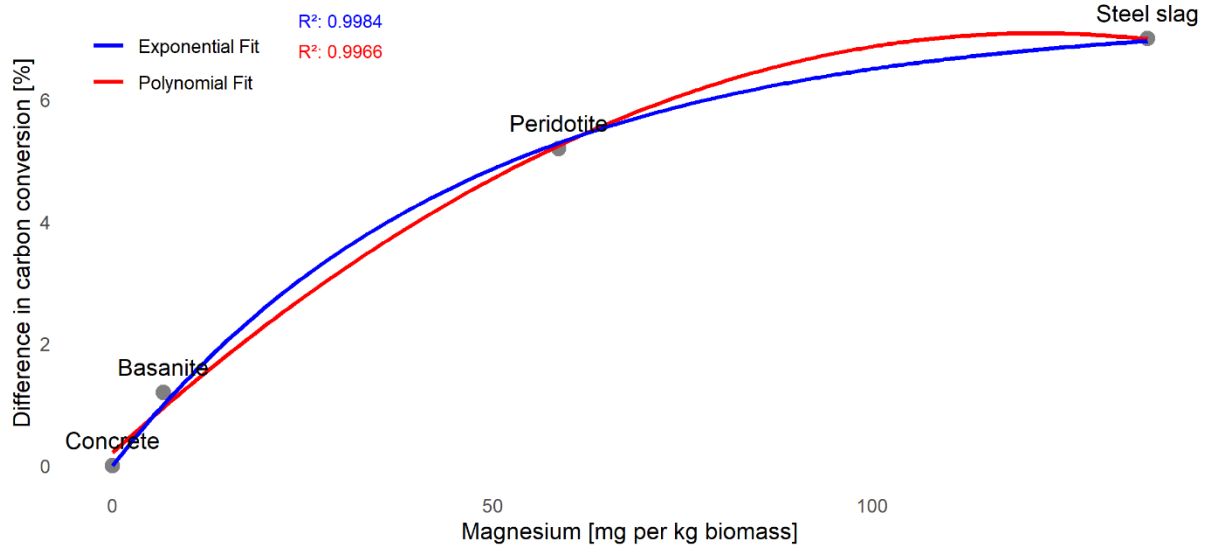


249

250 Figure S5: Absolute net values (control values were subtracted from soil amendments) of released major
 251 cations measured in the leachate water and exchangeable fraction at the end of the experiment. Negative
 252 values for leached cations indicate a retention in the soil, while negative values for the cation in the
 253 exchangeable fraction indicates a loss from the soil due to mineral dissolution. Calculations see S6,
 254 equations 15 and 16.

255

256 S9. Correlation of magnesium and carbon conversion from wet-impregnation



257

258 Figure S6. The exponential and polynomial fit of magnesium concentration in the mineral suspension and
259 the difference in carbon conversion of the resulting RE-biochars.

260

261 **S10. Description of qualitative assessment of soil amendments**

262 We applied a unified qualitative-scoring approach to compare all amendment configurations
 263 based on four key parameters: the experimental C-Sink, the geogenic IC-Sink, DOC leaching, and
 264 the additional preparation steps required for each material. To ensure consistency and
 265 comparability across these parameters, all measured values were converted into discrete scores
 266 ranging from -2 to +2, using percentile thresholds calculated across all configurations where the
 267 parameter was measurable (Table S3):

268 Table S3. Threshold for scoring of parameters.

Thresholds	Score	Experimental C-Sink	Geogenic IC-Sink	DOC leaching	Additional preparation steps
< 10 th percentile	-2	< 0.021	< -50.83%	< 14.07	wet-impregnation and pelletizing
10 th to 25 th percentile	-1	0.021 to 0.199	-50.83 to -23.17%	14.07 to 3.28	dry-mixing and pelletizing
25 th to 75 th percentile	0	0.199 to 0.979	-23.17 to 23.17%	3.28 to -3.28	-
75 th to 90 th percentile	1	0.979 to 1.023	23.17 to 50.83%	-3.28 to -14.07	mixing
> 90 th percentile	2	> 1.023	> 50.83%	> -14.07	no preparation

269

270 For the DOC leaching negative values (indicating DOC retention) were rated positive. We did not
 271 consider trace metal content and release as in one of the control soil columns thresholds for
 272 nickel and lead were exceeded by these columns. Some materials cannot express certain
 273 parameters (e.g., no PyC-Sink in single mineral amendments). These cases were assigned a
 274 neutral score of 0. The parameter “additional preparation steps” was evaluated qualitatively,
 275 with fewer preparatory requirements receiving higher scores and more complex treatments
 276 receiving lower scores. Cases in which a parameter could not be expressed for a given material
 277 configuration were assigned a neutral score of 0 and excluded from percentile calculations. The
 278 outcome of this assessment is displayed in Table S4.

279

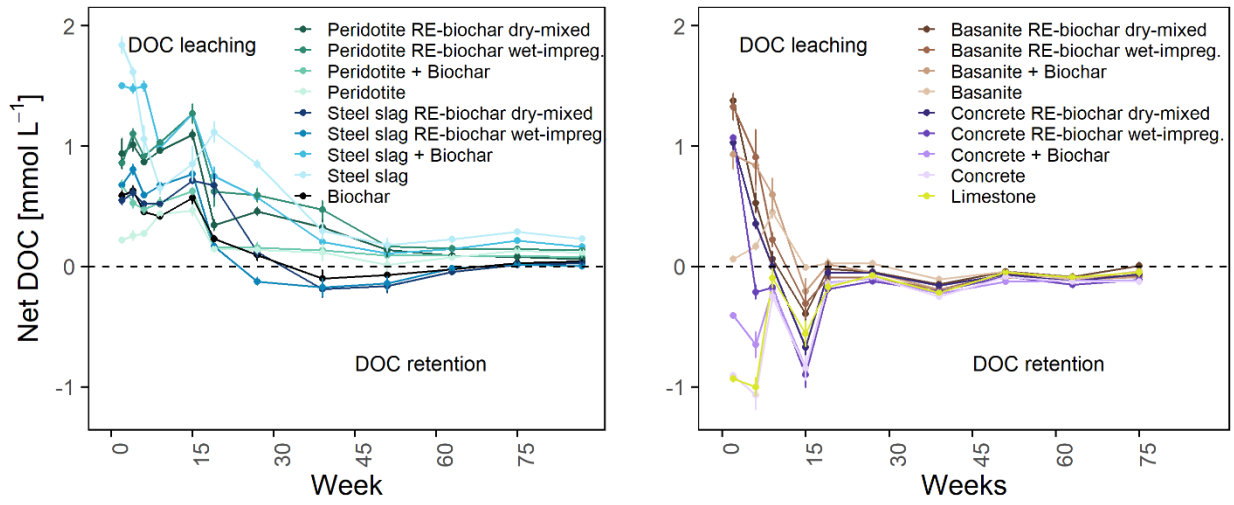
280

281 Table S4: Overview on the scoring of the main parameters that determined the rating of mineral and
 282 biochar combinations.

	Experimental C-Sink	Geogenic IC-Sink	DOC leaching	Additional preparation steps	Score	Recommendation
ConcreteChar-dry	0	-1	0	-1	-0.50	Co-application Single application
ConcreteChar-wet	0	-1	0	-2	-0.75	
Concrete + Biochar	2	0	1	1	1.00	
Concrete	-1		2	2	1.00	
SteelslagChar-dry	0	-1	-1	-1	-0.75	Co-application Single application
SteelslagChar-wet	0	-2	-1	-2	-1.25	
Steel slag + Biochar	1	-1	-2	1	-0.25	
Steel slag	-1		-2	2	-0.33	
BasaniteChar-dry	0	0	0	-1	-0.25	Co-application Single application
BasaniteChar-wet	0	0	-1	-2	-0.75	
Basanite + Biochar	1	1	0	1	0.75	
Basanite	-2		0	2	0.00	
PeridotiteChar-dry	0	2	-2	-1	-0.25	Co-application Single application
PeridotiteChar-wet	0	2	-2	-2	-0.50	
Peridotite + Biochar	1	1	-1	1	0.50	
Peridotite	-2		-1	2	-0.33	
Biochar	2		-1	2	1.00	
Limestone	-1		1	2	0.67	

283

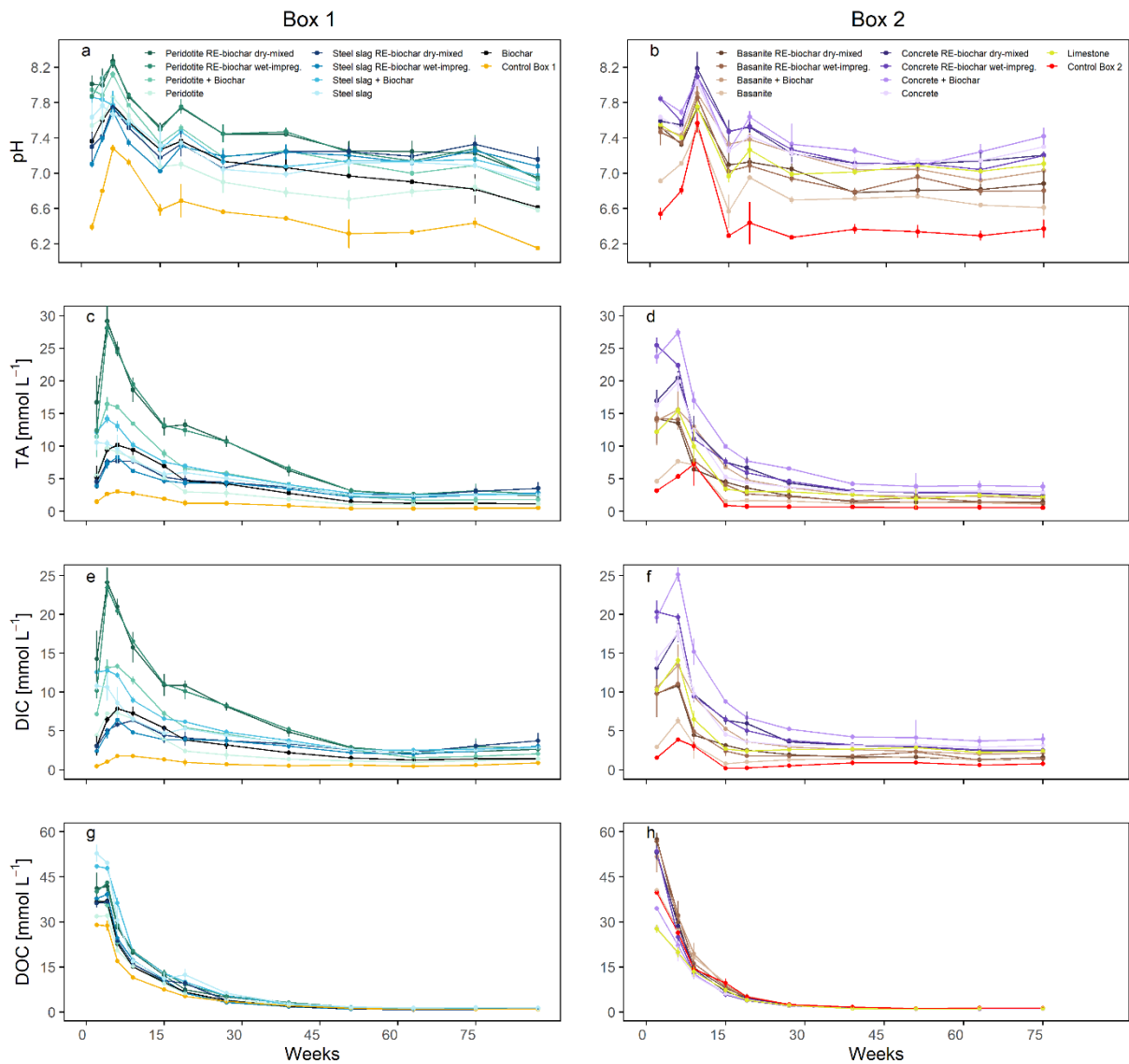
284 S11. Time series of net DOC fluxes, bulk chemistry, cations and anions
 285



286

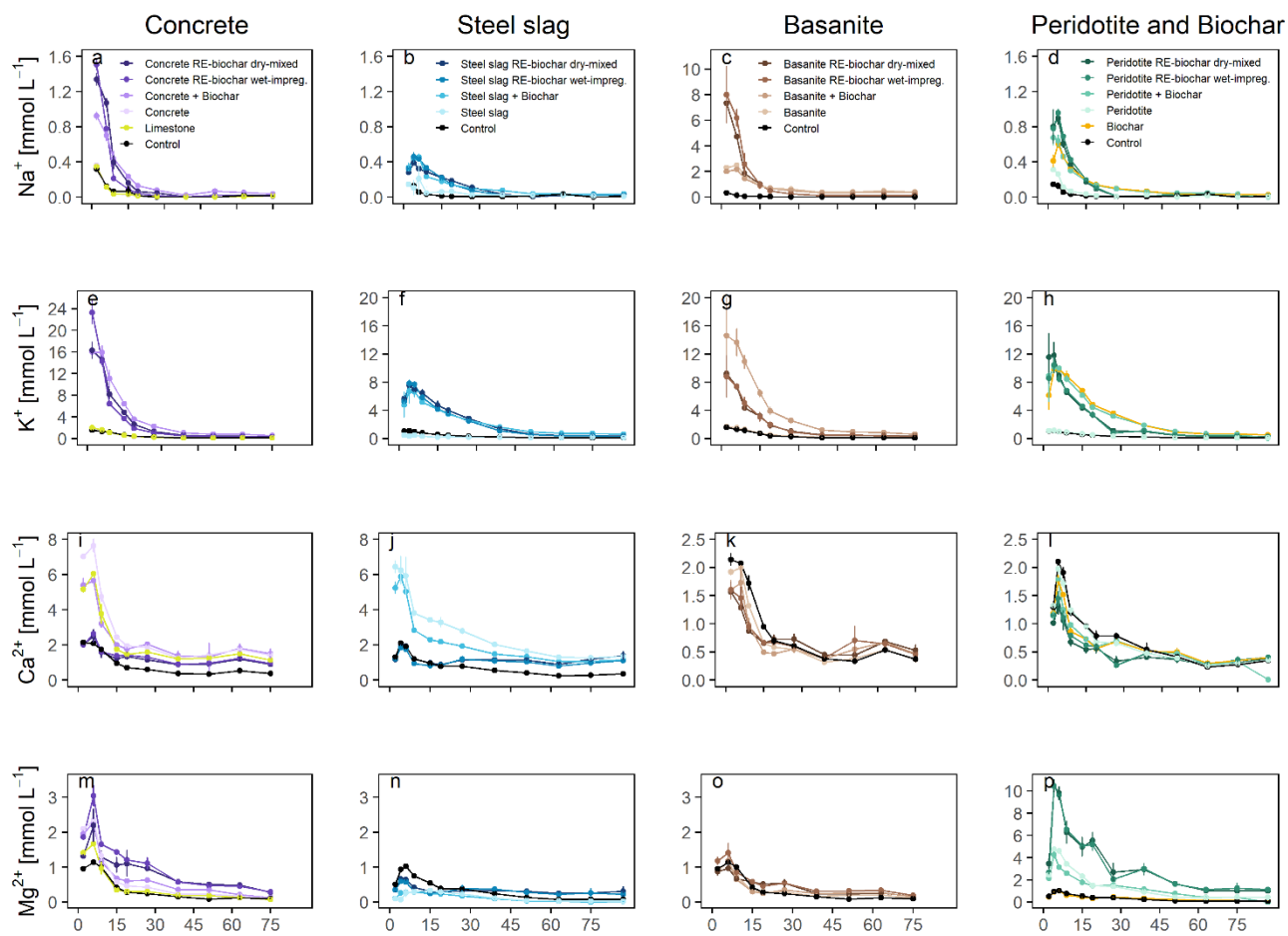
287 Figure S7. Time series of net DOC fluxes in the leachate water. Error bars indicate standard deviations
 288 (n=2).

289 S12. Time series of leachate analyses



290

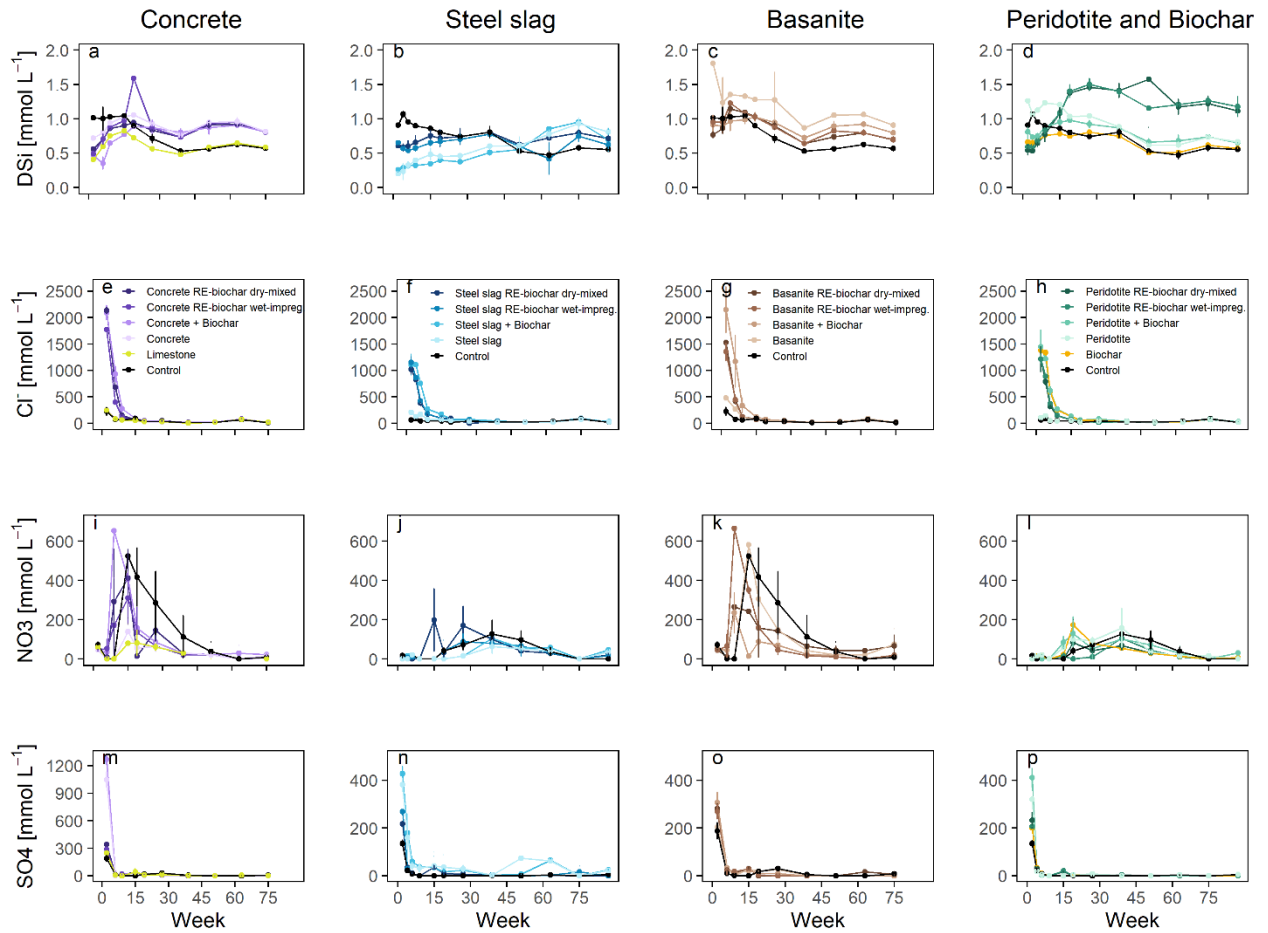
291 Figure S8. Time series of the bulk chemistry during the experiment with a-b) pH values, c-d) total
 292 alkalinity (TA), e-f) dissolved inorganic carbon (DIC), and dissolved organic carbon (DOC). Error bars
 293 indicate standard deviations (n=2).



294

295 Figure S9. Time series of major cations a-d) sodium (Na^+), e-h) potassium (K^+), i-l) calcium (Ca^{2+}), and

296 m-p) magnesium (Mg^{2+}). Error bars indicate standard deviations ($n=2$).



297

298 Figure S10. Time series of a-d) dissolved silica (DSi), e-h) chlorine (Cl⁻), i-l) nitrate (NO₃⁻), and m-p)
 299 sulphate (SO₄²⁻). Error bars indicate standard deviations (n=2).

300

301 **References**

- 302 Amann, T., Hartmann, J., Hellmann, R., Pedrosa, E.T., Malik, A., 2022. Enhanced
303 weathering potentials—the role of in situ CO₂ and grain size distribution.
304 *Front. Clim.* 4, 929268. <https://doi.org/10.3389/fclim.2022.929268>
- 305 Ansari, M., Stock, S., Dippold, M.A., Hamburger, S.E., Kammann, C.I., Meyer Zu
306 Drewer, J., Hagemann, N., Eschenbach, A., Becker, J.N., 2026. Biochar
307 dominated the combined effect of silicate rock powder and biochar
308 application on extracellular enzyme kinetics and nutrient dynamics in a
309 sandy soil. *Soil and Tillage Research* 262, 107234.
310 <https://doi.org/10.1016/j.still.2026.107234>
- 311 Dickson, A.G., 1981. An exact definition of total alkalinity and a procedure for the
312 estimation of alkalinity and total inorganic carbon from titration data. *Deep*
313 *Sea Research Part A. Oceanographic Research Papers* 28, 609–623.
314 [https://doi.org/10.1016/0198-0149\(81\)90121-7](https://doi.org/10.1016/0198-0149(81)90121-7)
- 315 Dietzen, C., Rosing, M.T., 2023. Quantification of CO₂ uptake by enhanced
316 weathering of silicate minerals applied to acidic soils. *International Journal*
317 *of Greenhouse Gas Control* 125, 103872.
318 <https://doi.org/10.1016/j.ijggc.2023.103872>
- 319 Hansen, H.P., Koroleff, F., 1999. Determination of nutrients, in: *Methods of*
320 *Seawater Analysis*. John Wiley & Sons, Ltd, pp. 159–228.
321 <https://doi.org/10.1002/9783527613984.ch10>
- 322 Meredith, W., McBeath, A., Ascough, P., Bird, M.I., 2017. Analysis of biochars by
323 hydropyrolysis (HyPy), in: Singh, B., Camps Arbestain, M., Lehmann, J.
324 (Eds.), . CRC Press, Clayton.
- 325 Parkhurst, D.L., Appelo, C.A.J., 2013. Description of input and examples for
326 PHREEQC version 3—A computer program for speciation, batch-reaction,
327 one-dimensional transport, and inverse geochemical calculations, in: *U.S.*
328 *Geological Survey Techniques and Methods*. U.S. Geological Survey,
329 Denver, p. 497.
- 330 Renforth, P., 2019. The negative emission potential of alkaline materials. *Nat*
331 *Commun* 10, 1401. <https://doi.org/10.1038/s41467-019-09475-5>
- 332 Rieder, L., Hagens, M., Poetra, R., Vidal, A., Calogiuri, T., Neubeck, A., Singh, A.,
333 Corbett, T., Niron, H., Vicca, S., Vlaeminck, S.E., Janssens, Iris, Verdonck, T.,
334 Janssens, Ivan, Li, X., Hammes, J.S., Hartmann, J., 2026. Contribution of
335 dissolved organic carbon to total alkalinity in Enhanced Weathering
336 experiments. *Applied Geochemistry* 198, 106685.
337 <https://doi.org/10.1016/j.apgeochem.2026.106685>

338 Schmidt, H.-P., Abiven, S., Hagemann, N., 2022. Permanence of soil applied
339 biochar. An executive summary for Global Biochar Carbon Sink
340 certification. *The Biochar Journal* 69–74.

341 Vorrath, M.-E., Amann, T., Meyer zu Drewer, J., Hagemann, N., Aldrich, C., Börker,
342 J., Seedtke, M., Becker, J.N., Hagens, M., Eschenbach, M., Hartmann, J.,
343 2025. Pyrogenic carbon and Carbonating Minerals for Carbon Capture and
344 Storage (PyMiCCS) Part II: Organic and Inorganic Carbon Dioxide Removal
345 in an Oxisol. *Frontiers in Climate*.
346 <https://doi.org/10.3389/fclim.2025.1592454>
347